© 2017. Published by The Company of Biologists Ltd | Development (2017) 144, 2837-2851 doi:10.1242/dev.150664

RESEARCH ARTICLE

Coup-TF1 and *Coup-TF2* control subtype and laminar identity of MGE-derived neocortical interneurons

Jia Sheng Hu*, Daniel Vogt, Susan Lindtner, Magnus Sandberg, Shanni N. Silberberg and John L. R. Rubenstein*

ABSTRACT

Distinct cortical interneuron (CIN) subtypes have unique circuit functions; dysfunction in specific subtypes is implicated in neuropsychiatric disorders. Somatostatin- and parvalbumin-expressing (SST^+ and PV^+) interneurons are the two major subtypes generated by medial ganglionic eminence (MGE) progenitors. Spatial and temporal mechanisms governing their cell-fate specification and differential integration into cortical layers are largely unknown. We provide evidence that *Coup-TF1* and *Coup-TF2* (*Nr2f1* and *Nr2f2*) transcription factor expression in an arc-shaped progenitor domain within the MGE promotes time-dependent survival of this neuroepithelium and the time-dependent specification of layer V SST^+ CINs. *Coup-TF1* and *Coup-TF2* autonomously repress PV^+ fate in MGE progenitors, in part through directly driving *Sox6* expression. These results have identified, in mouse, a transcriptional pathway that controls SST-PV fate.

KEY WORDS: Neurogenesis, Coup-TF1 (Nr2f1), Coup-TF2 (Nr2f2), Interneurons, Somatostatin, Parvalbumin, Mouse

INTRODUCTION

Cortical interneuron (CIN) subtypes play different roles in cortical computations through their distinct molecular properties, physiology and connectivity (Kepecs and Fishell, 2014). For example, parvalbumin-expressing (PV^+) fast-spiking, soma-innervating interneurons drive gamma oscillations, while somatostatin-expressing (SST^+) regular-spiking interneurons target pyramidal neuron dendrites, where they are crucial for sharpening stimuli intensity (Sohal et al., 2009; Murayama et al., 2009). Defects in interneuron subtypes may underlie some phenotypes of neuropsychiatric disorders, such as autism and schizophrenia (Marin, 2012).

A fundamental issue is how correct numbers (and ratios) of interneuron subtypes are generated and integrated into appropriate cortical layers. The mouse medial ganglionic eminence (MGE) produces most of the PV and SST interneurons, which represent about 40% and 30% of CINs, respectively (Xu et al., 2008). These numbers are controlled by regional, temporal and cell-type specification, differentiation and survival, and are regulated by cascades of transcription factors (TFs), including *Dlx1*, *Dlx2*, *Dlx5*, *Dlx6*, *Lhx6*, *Lhx8*, *Nkx2.1*, *Nkx6.2*, *Npas1*, *Npas3*, *Olig1*, *Satb1* and *Sox6* (Azim et al., 2009; Batista-Brito et al., 2009; Cobos et al., 2005; Colasante et al., 2008; Liodis et al., 2007; Sussel et al., 1999; Zhao et al., 2008). Non-transcription factors, such as *Ccnd2* (cyclin D2) and *Pten*, also control interneuron numbers (Glickstein et al., 2007; Vogt et al., 2015).

We focused on *Coup-TF2* (*Nr2f2*) function (steroid/thyroid hormone receptor superfamily member) because it, and its paralogue *Coup-TF1* (*Nr2f1*), are expressed in the MGE, and are largely confined to layer V SST^+ CINs (Cai et al., 2013; Lodato et al., 2011). Previous work on *Coup-TF1* and *Coup-TF2* in the embryonic basal ganglia focused on their function in the caudal ganglionic eminence (CGE) and amygdala (Lodato et al., 2011; Tang et al., 2012), although loss of *Coup-TF1* decreased SST/PV balance (Lodato et al., 2011). Here, through conditional mutagenesis, forced expression and transplantation we demonstrate that *Coup-TF2*, in conjunction with *Coup-TF1*, regulate cell cycle dynamics and cell fate decisions, including apoptosis, in MGE progenitors, but not in neurons. We show that *Coup-TF1* and *Coup-TF2* (*Coup-TF1/2*) function in a spatial- and temporal-specific manner to promote SST and repress PV interneurons. Furthermore, we provide evidence that *Coup-TF2* directs the development of layer V SST^+ interneurons, in part through driving *Sox6* expression via an enhancer element near the *Sox6* locus. Finally, we show that the caudal MGE is also a major source of SST^+ CINs.

RESULTS

Coup-TF2 loss in the Nkx2.1-Cre lineage reduces the neocortical SST^+/PV^+ interneuron ratio

COUP-TF2 expression in the MGE at E12.5 is highly graded, with prominent levels caudoventrally, extending towards the CGE and into the preoptic area (POA) where sonic hedgehog (*Shh*) expression in the VZ is present (Fig. 1A; Fig. S1H,I). Rostrally, COUP-TF2 is restricted to the rostral dorsal MGE (rdMGE), where it overlaps with *Nkx6.2* expression (Fig. S1G,H). Its graded expression is opposite to that of *Otx2*, which has a rostral-caudal gradient (Fig. S1B-E). High COUP-TF2 levels are also present in the CGE, caudoventral cortex and amygdala (Tang et al., 2012; Kanatani et al., 2008; Tripodi et al., 2004) (Fig. S15).

Coup-TF2 expression is complementary to *Nkx2.1* in the rdMGE and caudal MGE (cMGE) (Fig. S1H,J). We therefore hypothesized that *Nkx2.1* restricts *Coup-TF2* expression within the MGE. To test this, we compared *Coup-TF2* expression in E12.5 *Nkx2.1* conditional knockout mutants (*Olig2-Cre*$^+$*; Nkx2.1*$^{lox/lox}$) with littermate controls (*Olig2-Cre*$^+$*; Nkx2.1*$^{lox/+}$). Coup-TF2 expanded ventrally in the rostral MGE (Fig. S1K,K′) and its expression increased in the medial MGE (mMGE) (Fig. S1L,L′). These results indicate that *Nkx2.1* regionalizes *Coup-TF2* MGE expression.

We investigated *Coup-TF2* function in MGE- and POA-derived cells using conditional mutagenesis (Fig. S14A). Because *Coup-TF2* has overlapping functions with *Coup-TF1* (Tang et al., 2010), we sensitized the *Coup-TF2* mutants using a *Coup-TF1*$^-$ allele. Mutants were generated using the following cross: *Coup-TF1*$^{+/-}$*;*

Department of Psychiatry, Neuroscience Program and the Nina Ireland Laboratory of Developmental Neurobiology, University of California San Francisco, San Francisco, CA 94158, USA.

*Authors for correspondence (jia.hu@ucsf.edu; john.rubenstein@ucsf.edu)

J.S.H., 0000-0002-2530-2051; D.V., 0000-0003-1876-5936; S.N.S., 0000-0002-7979-9665; J.L.R.R., 0000-0002-4414-7667

Received 17 February 2017; Accepted 29 June 2017

Development (2017) 144, 2837-2851 doi:10.1242/dev.150664

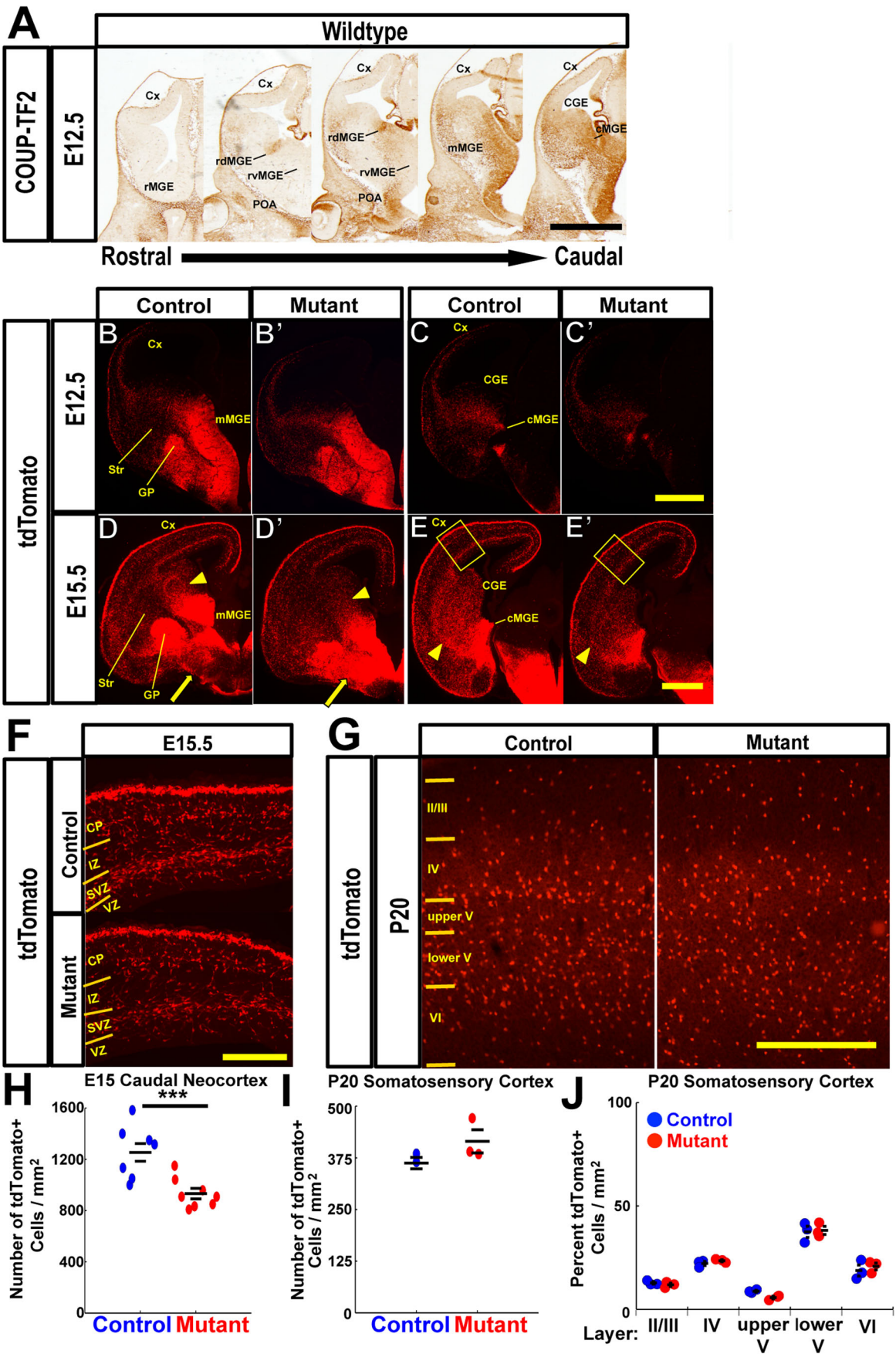

Fig. 1. See next page for legend.

Development (2017) 144, 2837-2851 doi:10.1242/dev.150664

Fig. 1. Embryonic expression of COUP-TF2 and its function in promoting CIN number (*Nkx2.1-Cre* lineage) in the prenatal caudal neocortex. (A) COUP-TF2 immunohistochemistry on a rostrocaudal series of coronal E12 wild-type hemisections (n=4). There is strong expression in rdMGE, mMGE and cMGE. Scale bar: 500 µm. (B-E′) Fate mapping of the *Nkx2.1-Cre* lineage in control and *Coup-TF2*-sensitized mutant. tdTomato immunohistochemistry on (B-C′) E12 (n=4 for each control and mutant) and (D-E′) E15 (n=8 for each control and mutant) control (*Nkx2.1-Cre*$^{+}$; *Coup-TF1*$^{+/-}$; *Coup-TF2*$^{lox/+}$; *Ai14*$^{lox/+}$) (B,C,D,E) and mutant (*Nkx2.1-Cre*$^{+}$; *Coup-TF1*$^{+/-}$; *Coup-TF2*$^{lox/lox}$; *Ai14*$^{lox/+}$) (B′,C′,D′,E′) coronal hemisections comparing expression of a Cre-dependent Ai14 reporter in two rostral-caudal planes, at the level of the mMGE and cMGE. Arrows in D,D′ indicate tdTomato accumulation in the MGE/POA MZ region in mutants. Arrowheads in D-E′ indicate tdTomato reduction in mutant LGE/CGE. Scale bars: 250 µm in C′; 500 µm in E′. (F) Magnified view of E15.5 neocortex (taken from the area outlined in yellow in E,E′). Scale bar: 100 µm. (G) tdTomato immunohistochemistry on P20 control (left panel) and mutant (right panel) somatosensory cortex (n=3 for each control and mutant). Scale bar: 500 µm. (H-J) tdTomato^{+} cell densities in control (blue) and mutant (red). (H) E15.5 caudal neocortex (all layers, from F); (I) P20 somatosensory cortex (from G, all layers); and (J) P20 tdTomato^{+} cell densities in each layer of the somatosensory cortex. Data are mean±s.e.m. Student's t-test (except for J, where χ^2 test was used). ***P<0.001. CP, cortical plate; CGE, caudal ganglionic eminence; Cx, cortex; IZ, intermediate zone; cMGE, caudal medial ganglionic eminence; mMGE, middle medial ganglionic eminence; rMGE, rostral medial ganglionic eminence; rdMGE, rostral dorsal medial ganglionic eminence; rvMGE, rostral ventral medial ganglionic eminence; POA, preoptic area; Str, striatum; SVZ, subventricular zone; VZ, ventricular zone.

Coup-TF2 $^{lox/lox}$; *Ai14*$^{lox/lox}$ females×*BAC-Nkx2.1-Cre*$^{+}$; *Coup-TF2* $^{lox/+}$ males. Henceforth, we refer to *Nkx2.1-Cre*$^{+}$; *Coup-TF1*$^{+/-}$; *Coup-TF2*$^{lox/lox}$; *Ai14*$^{lox/+}$ as the *Coup-TF2*-sensitized mutants, unless specified otherwise. Controls were *Nkx2.1-Cre*$^{+}$; *Coup-TF1*$^{+/-}$; *Coup-TF2*$^{lox/+}$; *Ai14*$^{lox/+}$. The sensitized mutants were viable postnatally. Qualitatively, non-sensitized and sensitized *Coup-TF2* mutants had the same phenotypes; reducing *Coup-TF1* dose increased phenotype severity.

We first studied the effect of the *Coup-TF2* mutation on MGE patterning by examining the expression at E12.5 of *Nkx6.2*, *Otx2* and *Shh*. *Nkx6.2* expression, a marker of the rdMGE [which is where some SST^{+} CINs originate (Fogarty et al., 2007; Sousa et al., 2009)], was unchanged (Fig. S1N,N′). *Otx2* and *Shh* expression, markers of the rostral MGE and ventral MGE, respectively, also did not change (Fig. S1M,M′,O,O′). Therefore, no defect in MGE patterning was found in the *Coup-TF2*-sensitized mutant.

We then followed the fate of MGE-POA cells using *Nkx2.1-Cre* lineage analysis and the *Ai14* (tdTomato) Cre recombination reporter. At E12.5, we detected a reduction in tdTomato^{+} cells coming out of the cMGE but not in the mMGE (Fig. 1B-C′). By E15.5, there were more tdTomato^{+} cells in the POA, and fewer cells migrating through the lateral ganglionic eminence (LGE) and CGE from the mMGE and cMGE, and into the piriform cortex and globus pallidus (GP) (Fig. 1D-E′). The caudal neocortex had 30% fewer tdTomato^{+} cells (Fig. 1F,H), whereas the rostral neocortex appeared normal. By P20, neocortical fate map analysis showed no obvious phenotype (Fig. 1G,I,J; Fig. S12A), including in layer V, where most MGE-derived COUP-TF2^{+} cells are located (Cai et al., 2013). Thus, *Coup-TF2*-sensitized mutants had a transient decrement of *Nkx2.1-Cre* lineage cells migrating to the neocortex.

CINs in the *Coup-TF2*-sensitized mutants had a decreased SST^{+}/PV^{+} ratio at P20 (Fig. 2A,B). This was due to a 22.0% reduction in SST^{+} CIN density. This decrease mainly occurred in the lower part of layer V (Fig. 2C). In contrast, the PV^{+} CIN density was increased, with changes occurring in layers II/III, IV and VI (Fig. 2A-C; Fig. S12A).

Next, we examined whether SST^{+} CIN numbers and laminar distribution were affected at P0 in *Coup-TF1/Coup-TF2* double mutants (2% of *Coup-TF1*$^{-/-}$ survive after P0; Qiu et al., 1997) (*Nkx2.1-Cre*$^{+}$; *Coup-TF1*$^{-/-}$; *Coup-TF2*$^{lox/lox}$). SST^{+} CIN density was reduced by ∼30% (Fig. S2A,B). The ratio of SST^{+} CINs in deep layers (V, VI) versus cortical plate (CP) decreased by 85% (Fig. S2A,C; Fig. S12B). Thus, the SST^{+} CIN number and laminar positioning defects occurred as early as P0.

We examined SST^{+} cell numbers in *Coup-TF2*-sensitized mutants at prenatal ages to determine the onset of SST reduction. There was a reduction in SST^{+} cells migrating into the neocortex at E12.5, an age when *Sst* expression was first observed, and at E17.5 (Fig. 2D-F, Fig. S3A-C). At E12.5, the reduction was clearest in caudal regions (Fig. 2E,E′,G), consistent with *Coup-TF2* expression in the cMGE (Fig. 1A).

We examined prenatal expression of known regulators of MGE-derived CIN development. At E12.5, *Nkx2.1* expression was unchanged in the basal ganglia (Fig. S3D,E). *Lhx6* and *Sox6* expression, TFs that promote SST^{+} fate (Azim et al., 2009; Batista-Brito et al., 2009; Zhao et al., 2008; Vogt et al., 2014), was decreased in tangentially migrating interneurons (Fig. S3F,G), and in the SVZ and MZ of the caudal MGE (Fig. 7A,B), respectively. At E17.5, *Npas1* expression was reduced, a TF that marks SST^{+} but not PV^{+} interneurons (Fig. S3H,I) (Stanco et al., 2014). Therefore, at E12.5 *Coup-TF2*-sensitized mutants generated fewer immature interneurons expressing *Sst*, *Lhx6* and *Sox6*.

To determine whether the SST phenotype is also present when *Coup-TF2* function is removed from MGE SVZ progenitors, we used the *Dlx1-CreERT* allele. Embryos exposed to tamoxifen at E10.5 (harvested at E13.5) and at E12.5 (harvested at E15.5) showed decreased *Sst* expression in the neocortex (Fig. 3A,A′) and decreased numbers of cells migrating through the LGE (Fig. 3B,B′), respectively.

To test *Coup-TF2* function in postmitotic MGE-derived neurons, we used the *Somatostatin-IRES-Cre* allele, the expression of which begins at ∼E12.5 (Taniguchi et al., 2011) (Fig. S14B). Analysis comparing *Somatostatin-IRES-Cre*$^{+}$; *Coup-TF1*$^{+/-}$; *Coup-TF2*$^{lox/lox}$; *Ai14*$^{lox/+}$ (mutant) with *Somatostatin-IRES-Cre*$^{+}$; *Coup-TF1*$^{+/-}$; *Coup-TF2*$^{lox/+}$; *Ai14*$^{lox/+}$ (control) at P20 in the somatosensory cortex found no change in the number of tdTomato^{+}, SST^{+} or PV^{+} cells, and the lamination of SST^{+} CINs (Fig. 3C-J). Thus, *Coup-TF2* regulates the SST^{+}/PV^{+} ratio and laminar identity in MGE/POA progenitors, but not in neurons.

Coup-TF2 regulates basal ganglia histogenesis and cholinergic neuron development

As shown in the Ai14 fate-mapping experiments, the *Coup-TF2*-sensitized mutation disrupted basal ganglia histogenesis (Fig. 1D, E). Gene expression analyses at E12.5 of TFs that regulate these structures showed no changes in *Nkx2.1* and *Lhx6* expression (Fig. S3D-G). However, by E15.5, *Nkx2.1*, *Lhx6* and *Lhx8* expression provided evidence for a hypoplastic GP and excessive ventral MGE/POA cells, consistent with the E15.5 Ai14 fate mapping (Fig. S4B-E). Because of the ventral MGE/POA defect, we examined differentiation of choline acetyltransferase (ChAT^{+}) neurons that are derived from this region (Hoch et al., 2015a,b), by assessing *Gbx2* and *Lhx8* expression, which are TF regulators of these neurons (Chen et al., 2010; Zhao et al., 2003). Striatal interneuron expression of *Gbx2* and *Lhx8* was reduced at E15.5 and E17.5 (Fig. S4D-K), as was P0 expression of the ChAT-neuron marker *TrkA* (*Ntrk1*) (Fig. S4L,M) and P20 expression of ChAT (Fig. S4N,O). Thus, *Coup-TF2* was required for the expression of *Sox6*, *Lhx6* and *Npas1* (regulators of MGE/POA-derived cortical GABAergic interneurons), and

Development (2017) 144, 2837-2851 doi:10.1242/dev.150664

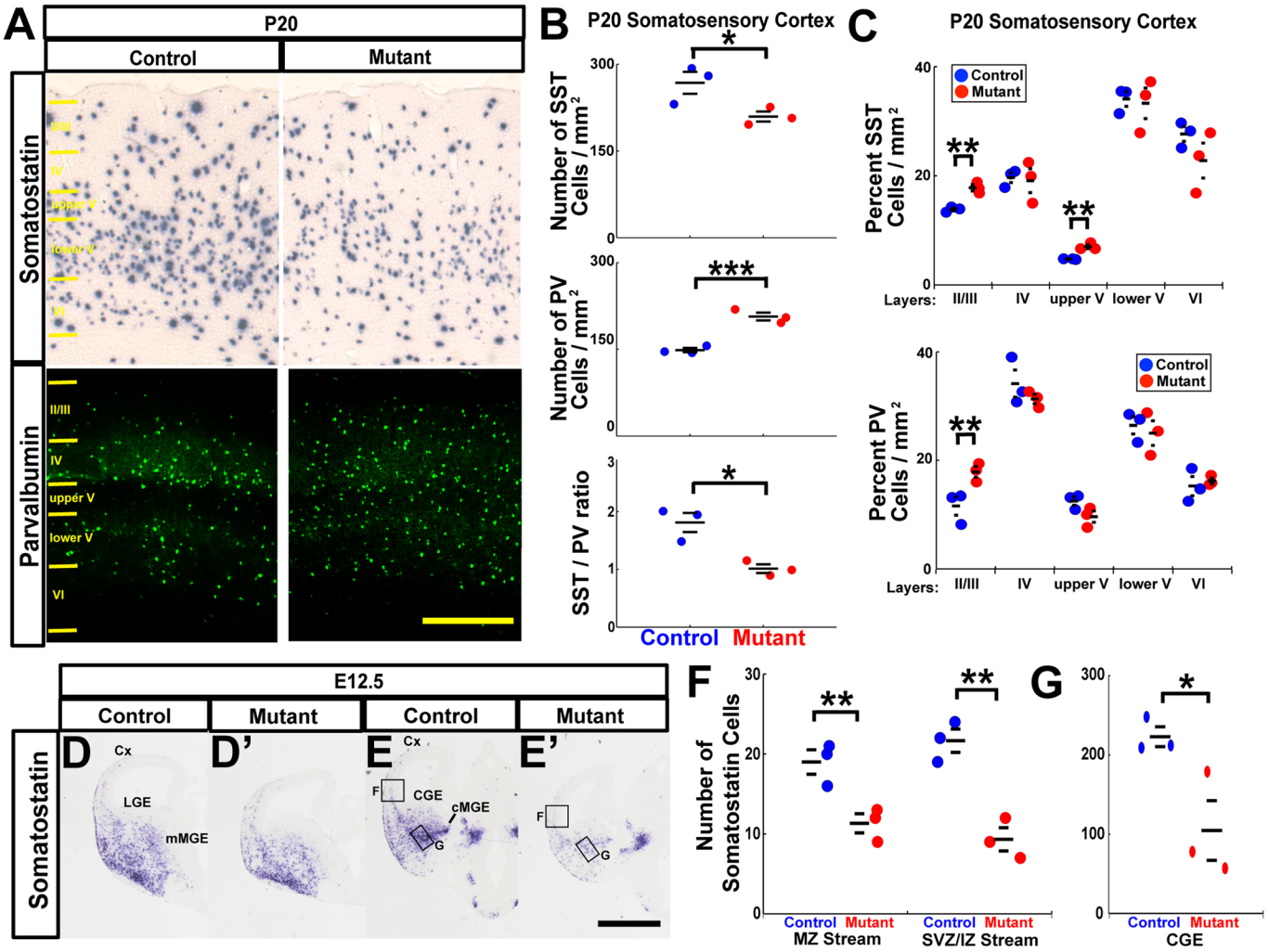

Fig. 2. *Coup-TF2*-sensitized mutants generate fewer SST CINs and have a reduced SST$^+$/PV$^+$ ratio in P20 somatosensory cortex. (A) *Sst in situ* hybridization (top panels) (*n*=3 for each control and mutant) and PV immunohistochemistry (bottom panels) (*n*=3 for each control and mutant) on P20 control (left column) and mutant (right column) somatosensory cortices. Scale bar: 500 µm. (B) SST$^+$ (top panel) and PV$^+$ (middle panel) cell density quantifications, and the SST$^+$/PV$^+$ ratio (bottom panel) for all layers in control (blue) and mutant (red) P20 somatosensory cortices. (C) SST$^+$ (top panel) and PV$^+$ (bottom panel) cell quantifications in each layer of control (blue) and mutant (red) P20 somatosensory cortices. (D-E′) *Sst in situ* hybridization on E12.5 control (D,E) and *Coup-TF2*-sensitized mutant (D′,E′) coronal hemisections in two rostral-caudal planes (at the level of the mMGE and cMGE) (*n*=3 for each control and mutant). Scale bar: 1 mm. (F,G) SST$^+$ cell quantifications in the cortical MZ and SVZ (F) (counted from boxes in Cx from E,E′), and in CGE (G) (counted from boxes in CGE from E,E′), from control (blue) and mutant (red) brains. Data are mean±s.e.m. Student's *t*-test (except for C where χ^2 test was used). **P*<0.05; ***P*<0.01; ****P*<0.001. CGE, caudal ganglionic eminence; cMGE, caudal medial ganglionic eminence; Cx, cortex; LGE, lateral ganglionic eminence.

Gbx2, *Lhx8*, *TrkA* and ChAT (regulators of striatal cholinergic interneurons).

Coup-TF2 loss in the Nkx2.1-Cre lineage results in an increase in apoptosis

Apoptosis could be responsible for reduced numbers of SST$^+$ CINs and ChAT$^+$ striatal interneurons in *Coup-TF2*-sensitized mutants. As these decreases were first detected at E12.5, we assayed for cleaved-caspase 3 (cC3) at E11.5, E12.5 and E13.5. At E11.5, we detected cC3$^+$ cells in the VZ, SVZ1 and SVZ2 of the rdMGE and cMGE, where COUP-TF2 is expressed (Fig. 4A; Fig. S5A). At E12.5, cC3$^+$ cells persisted in the rdMGE VZ, SVZ1 and SVZ2, but not in the cMGE (Fig. 4A; Fig. S5A). At E13.5, cC3$^+$ cells were not detected in either MGE region. Moreover, few cC3$^+$ cells were observed in the COUP-TF2-negative rostral ventral MGE (rvMGE) (Fig. 4A; Fig. S5A). Thus, cells from *Coup-TF2*-sensitized mutant rdMGE and cMGE (*Coup-TF2*$^+$ zones) are susceptible to apoptosis within a restricted time window.

Coup-TF2 loss in the *Nkx2.1-Cre* lineage results in premature neurogenesis

We next determined whether impaired neurogenesis also contributed to decreased SST$^+$ interneuron numbers in *Coup-TF2*-sensitized mutants. To measure neurogenesis, we counted the fraction (Q fraction) of newly postmitotic EdU$^+$ cells (five hours after EdU administration) that were β-III-tubulin (TuJ1$^+$, pan-neuronal marker). At E11.5, the Q fraction increased in *Coup-TF2*-sensitized mutants in the VZ and SVZ1 of the rdMGE and cMGE (Fig. 4B; Fig. S5B). At E12.5, the Q fraction remained higher in the sensitized mutant than control in rdMGE SVZ1 but decreased in SVZ1 and SVZ2 of the cMGE. The Q fraction was not altered in the *Coup-TF2*$^-$ rvMGE at E11.5 and E12.5 (Fig. 4B; Fig. S5B).

Development (2017) 144, 2837-2851 doi:10.1242/dev.150664

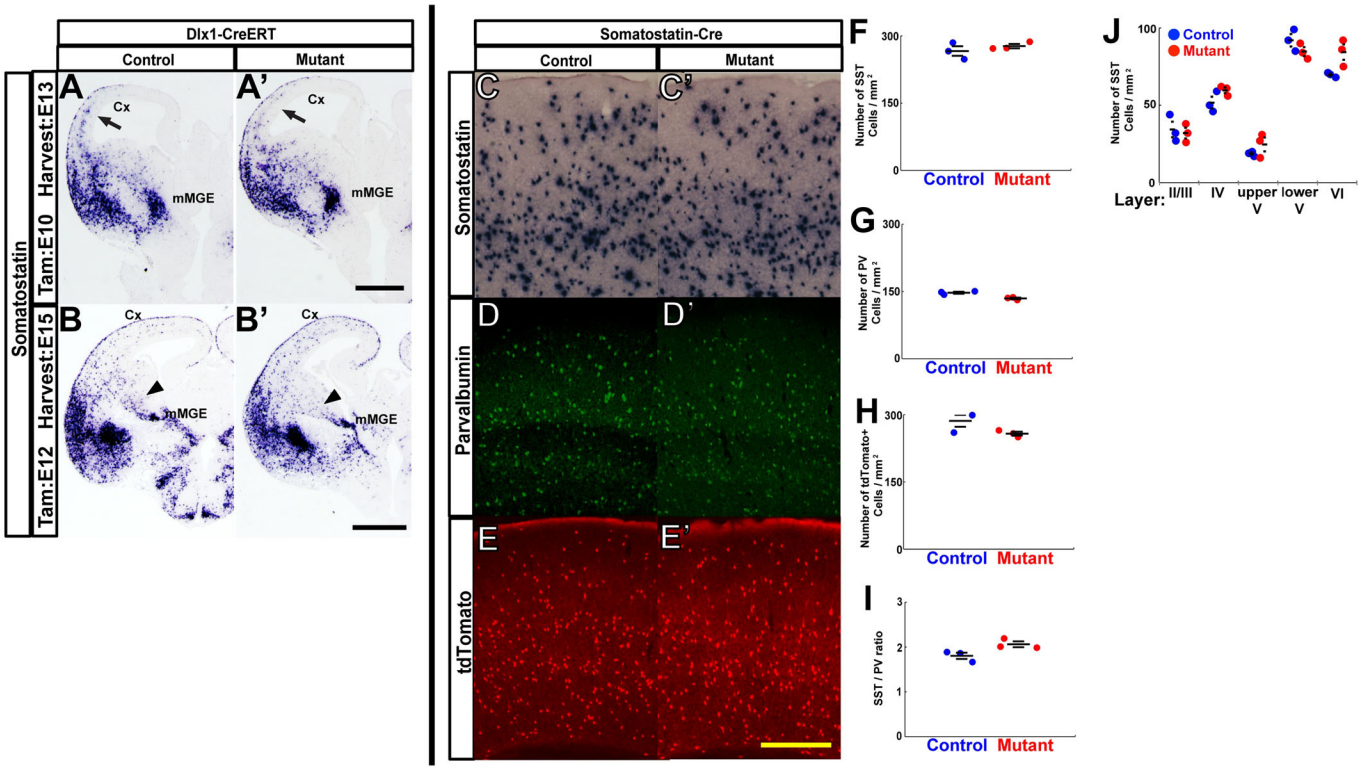

Fig. 3. *Coup-TF2* regulates SST$^+$ interneuron number and laminar identity in progenitors but not in neurons. (A-B′) *Sst in situ* hybridization on (A,A′) E13 (tamoxifen E10) (*n*=3 for each control and mutant; experiment replicated twice) or (B,B′) E15 (tamoxifen E12) (*n*=3 for each control and mutant; experiment replicated twice) control (*Dlx1-CreERT*$^+$*; Coup-TF1*$^{+/-}$*; Coup-TF2*$^{lox/+}$) (A,B) and mutant (*Dlx1-CreERT*$^+$*; Coup-TF1*$^{+/-}$*; Coup-TF2*$^{lox/lox}$) (A′,B′) coronal hemisections. Arrows indicate reduced *Sst* expression in mutant cortex (A,A′). Arrowheads indicate reduced *Sst* expression in mutant mMGE (B,B′). Scale bars: 1 mm in A′; 500 µm in B′. (C-E′) *Sst in situ* hybridization (C,C′) (*n*=3 for each control and mutant), PV immunohistochemistry (D,D′) (*n*=3 for each control and mutant) and tdTomato immunohistochemistry (E,E′) (*n*=3 for each control and mutant) on P20 control (*SST-IRES-Cre*$^+$*; Coup-TF1*$^{+/-}$*; Coup-TF2*$^{lox/+}$*; Ai14*$^{lox/+}$) (C-E) and mutant (*SST-IRES-Cre*$^+$*; Coup-TF1*$^{+/-}$*; Coup-TF2*$^{lox/lox}$*; Ai14*$^{lox/+}$) (C′-E′) somatosensory cortices. tdTomato$^+$ cell numbers reflect the amount of SST-IRES-Cre lineage cells expressing Cre-dependent tdTomato reporter (Ai14). Scale bar: 500 µm. (F-H) *Sst*$^+$ (F), PV$^+$ (G) and dsRed$^+$ (H) cell density quantifications for all layers in control (blue) and mutant (red) P20 somatosensory cortices. (I) SST$^+$/PV$^+$ ratios in control (blue) and mutant (red) P20 somatosensory cortices. (J) SST$^+$ cell densities in each layer of control (blue) and mutant (red) P20 somatosensory cortices. Data are mean±s.e.m. Student's *t*-test. Cx, cortex; mMGE, middle medial ganglionic eminence.

The increased Q fraction seen at E11.5 in the rdMGE and cMGE could be artificially due to progenitors undergoing apoptosis. We therefore assessed if the cC3$^+$ cells in *Coup-TF2*-sensitized mutants were progenitors or differentiated cells. We found that ∼70% of cC3$^+$ cells were TuJ1$^-$; therefore, most of these dying cells were progenitors (Fig. 4C). While this can inflate the Q fraction, the significant increase in TuJ1$^+$ neurons in the VZ and SVZ1 of the rdMGE and cMGE (13.5±1.44 in control versus 25.0±0.82 in *Coup-TF2*-sensitized mutant) provides evidence for precocious neurogenesis.

Coup-TF2 loss in the Nkx2.1-Cre lineage results in increased proliferation

Precocious neurogenesis and apoptosis could be due to abnormal cell cycle dynamics. To explore this possibility, we counted the number of S- and M-phase cells (EdU$^+$ following a 5 h pulse and pH3$^+$, respectively). There were no changes in EdU$^+$ and pH3$^+$ cell numbers at E11.5, the age with precocious differentiation and apoptosis. Changes in proliferation were first detected at E12.5, with increases in EdU$^+$ cells in the rdMGE and cMGE SVZ1 (Fig. 4D; Fig. S5C), and in pH3$^+$ cells in the rdMGE and cMGE SVZ1 and SVZ2 (Fig. 4E; Fig. S5D). These increases persisted at E13.5 in the rdMGE and cMGE SVZ1. In the VZ, pH3$^+$ cell numbers only changed at E12.5, with decreases in the rdMGE and cMGE, whereas EdU$^+$ cell numbers did not change at any age.

We next assessed expression of *Ccnd2*, a promoter of G_1 progression (Glickstein et al., 2007). *Coup-TF2*-sensitized mutants had increased *Ccnd2* expression in the SVZ of the rdMGE and cMGE (Fig. 4F,G). These results indicate an increase number of rdMGE and cMGE progenitors remaining in cell cycle in *Coup-TF2*-sensitized mutants. Although we did not find evidence for this based on EdU-labeling P-fraction analyses (Fig. S11), the increase in E12.5 pH3$^+$ and EdU$^+$ in SVZ1 (described above) is consistent with increased SVZ1 proliferation that supports more neurogenesis of later-born MGE-derived neurons. Indeed, in the mutants we observed increased numbers of CINs that are born at E14.5 (Fig. 5D), and a recovery in the number of *Lhx6*$^+$ CINs at E17.5 (Fig. S6). Furthermore, the mutants had a normal number of neocortical *Nkx2.1-Cre* lineage cells by P20 (Fig. 1B-J), providing additional evidence for a recovery of CIN output.

Coup-TF2 loss in the *Nkx2.1-Cre* lineage has distinct temporal effects on PV$^+$ and SST$^+$ neurons

Because *Coup-TF2* loss in MGE/POA progenitors has temporally specific alterations in cell cycle dynamics (Fig. 4), we next studied the effect of the mutation on neuronal output from different ages. We used EdU incorporation to follow the fate and location of the tdTomato$^+$ MGE/POA-derived cells that had become postmitotic

Development (2017) 144, 2837-2851 doi:10.1242/dev.150664

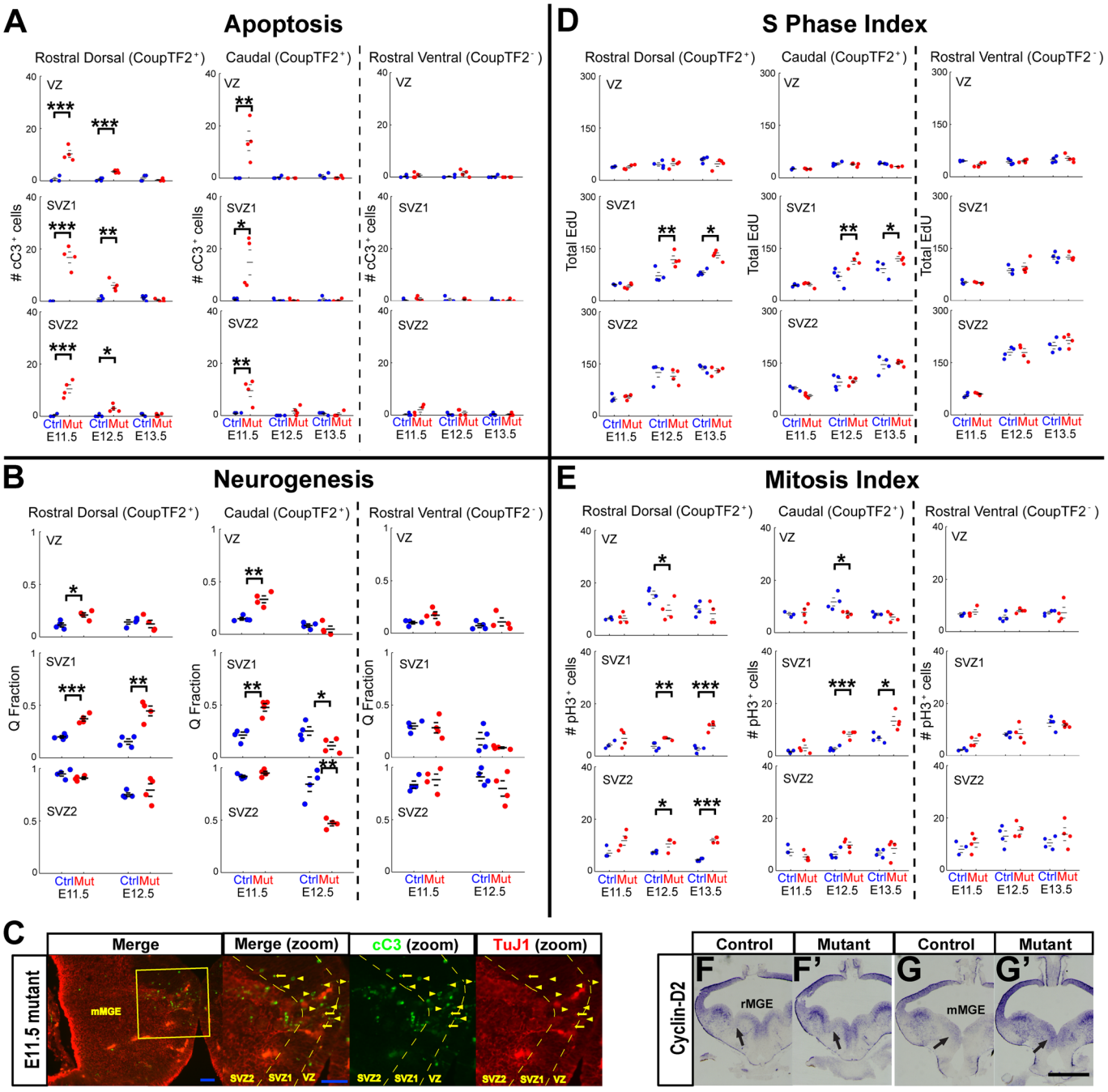

Fig. 4. *Coup-TF2* regulates the cell cycle in the MGE, neurogenesis and survival in a spatial- and temporal-dependent manner. (A,B,D,E) Quantification of (A) cC3$^+$ cells (n=4 for each control and mutant for each age), (B) total EdU$^+$ cells that are TuJ1$^+$ (Q fraction; newly generated neurons) (n=4 for each control and mutant for each age; experiment replicated three times for each age), (D) total EdU (S-phase marker) (n=4 for each control and mutant for each age; experiment replicated three times for each age) and (E) pH3$^+$ cells (M-phase marker) (n=4 for each control and mutant for each age) in VZ (top row), SVZ1 (middle row) and SVZ2 (bottom row) of the rdMGE (left column, CoupTF2$^+$), cMGE (middle column, CoupTF2$^+$) and rostral ventral MGE (right column, CoupTF2$^-$) at E11.5, E12.5 and E13.5 (except B). Data are from control (blue) and *CoupTF2*-sensitized mutant (red). (C) The first panel shows merged images taken in *Coup-TF2*-sensitized mutant mMGE of cC3 (green) and TuJ1 (red) immunohistochemistry on E11.5 coronal sections. The second panel shows a magnified view from the area outlined in the first panel. Individual cC3 and TuJ1 images are shown in third and fourth panels, respectively. Yellow arrowheads indicate apoptotic progenitors (cC3$^+$/TuJ1$^-$). Yellow arrows indicate apoptotic neurons (cC3$^+$/TuJ1$^+$). Scale bars: 50 µm. (F-G′) *Ccnd2 in situ* hybridization on E12.5 control (F,G) and *Coup-TF2*-sensitized mutant (F′,G′) coronal hemisections in two rostral-caudal planes; rostral and middle MGE levels (n=3 for each control and mutant). Arrows indicate increased *Ccnd2* expression in mutant MGE SVZ. Scale bar: 1 mm. Data are mean±s.e.m. Student's t-test. *P<0.05; **P<0.01; ***P<0.001. [Also see Fig. S5.] mMGE, middle medial ganglionic eminence; rMGE, rostral medial ganglionic eminence; SVZ1, subventricular zone 1; SVZ2, subventricular zone 2; VZ, ventricular zone.

(EdU$^+$) at different times. We introduced EdU into pregnant mice at E11.5, E12.5 or E14.5, and determined the density of cells double-labeled with tdTomato$^+$ (driven by *Nkx2.1Cre*) and EdU$^+$ in different telencephalic regions at P20. We also used immunohistochemistry to examine PV$^+$ and SST$^+$ neuron expression in the EdU$^+$ cells, to assess whether specific subtypes

Development (2017) 144, 2837-2851 doi:10.1242/dev.150664

of MGE/POA-derived neurons, with distinct birthdates, were differentially affected in the *Coup-TF2*-sensitized mutants.

Mutants had an increased density of MGE/POA (tdTomato$^+$)-derived cells born at E11.5 (EdU$^+$) in the somatosensory cortex, piriform cortex, globus pallidus and magnocellular preoptic (MCPO) (Fig. 5D-H, Fig. S7). This was associated with an increased number of PV$^+$ neurons (except in the MCPO). An E11.5 birthdate corresponds to the time when the mutant had precocious neurogenesis (Fig. 4B). The numbers of SST$^+$ neurons born at E11.5 did not change.

The density of MGE/POA-derived mutant cells born at E12.5 increased in the globus pallidus (Fig. 5H; Fig. S7), but decreased in somatosensory cortex and striatum (Fig. 5D,F; Fig. S7). Decreased SST$^+$ somatosensory cortex interneuron numbers was associated with this reduction (Fig. 5D; Fig. S7). Although SST$^+$ and PV$^+$ neuron numbers did not change in the striatum, the reduction in striatal MGE/POA-derived cells may be accounted for by the decline in cholinergic striatal interneurons (Fig. S4).

Finally, there were increased densities of cells born at E14.5 in the somatosensory cortex, piriform cortex and striatum (Fig. 5D-F; Fig. S7). These increases were associated with the increased numbers of PV$^+$ cells born at E14.5. SST$^+$ neuron numbers did not change (Fig. 5D-F; Fig. S7).

Thus, EdU fate-mapping analyses found: (1) that increases in cells born at E11.5 contributed to pallidal projection neurons [globus pallidus (PV$^+$) and MCPO], and PV$^+$ interneurons in the piriform cortex and somatosensory cortex; (2) that decreases in cell numbers were found only if they became postmitotic at ∼E12.5; these cells were SST$^+$ interneurons in the somatosensory cortex and piriform cortex; and (3) increases in the number of cells born at ∼E14.5 in the somatosensory cortex, piriform cortex and striatum; these cells were PV$^+$. Thus, *Coup-TF2* differentially regulates subtype identities of MGE/POA-derived neurons based on their birthdates.

Rostral and caudal MGEs generate inverse SST$^+$/PV$^+$ ratios of CINs

While premature neurogenesis and apoptosis may contribute to the decreased SST$^+$/PV$^+$ ratio in *Coup-TF2*-sensitized mutants, it does not rule out the possibility that *Coup-TF2* functions cell-autonomously as a regulator of SST versus PV fate. We used the MGE-to-cortex transplantation assay to study *Coup-TF2* function in CIN fate, as we had done to study *Lhx6* function (Vogt et al., 2014). Because *Coup-TF2* is preferentially expressed in the cMGE (Fig. 1), we compared the SST$^+$/PV$^+$ ratio from E12.5 transplanted cMGE and rostral MGE.

Transplanted interneurons were tdTomato$^+$ (driven by *Nkx2.1-Cre*). At 27 days post-transplantation (DPT), we assayed tdTomato co-expression with SST and PV. The SST$^+$/PV$^+$ ratio was higher (5.5±0.6) from the cMGE than the rostral MGE (1.4±0.2) (blue, Fig. 6D). Correspondingly, cMGE transplants had more SST and less PV interneurons than rostral MGE transplants (blue, Fig. 6B,C; Fig. S8A,B). Thus, E12.5 cMGE preferentially generated SST interneurons, consistent with our genetic evidence, supporting the idea that *Coup-TF2* promotes the generation of SST$^+$ and represses PV$^+$ interneuron fate (Fig. 2).

Coup-TF2 loss in cMGE, but not in rostral MGE, decreased the SST$^+$/PV$^+$ ratio

Next, we used the MGE transplantation assay to compare the effect of the *Coup-TF2*-sensitized mutation on the SST$^+$/PV$^+$ ratio from the rostral and caudal MGE. Although loss of *Coup-TF2* did not affect the SST$^+$/PV$^+$ ratio from the rostral MGE, the *Coup-TF2*-sensitized mutation reduced the SST$^+$/PV$^+$ ratio by 85% from the cMGE (Fig. 6D; Fig. S8A-D). The transplantation assay provided evidence that *Coup-TF2* cell-autonomously regulated the SST$^+$/PV$^+$ ratio. Moreover, because the SST$^+$/PV$^+$ ratio in the transplanted rostral and caudal *Coup-TF2*-sensitized mutant MGEs were similar, this suggests that *Coup-TF2* is a key mechanism for 'caudalizing' the MGE.

Coup-TF2 overexpression in MGE cells increases the SST$^+$/PV$^+$ ratio

To further test the hypothesis that *Coup-TF2* autonomously regulates the SST$^+$/PV$^+$ fate choice, we used lentiviral transduction (*DlxI12b-Cre-T2a-Coup-TF2*) to ectopically express *Coup-TF2* in the MGE. The *DlxI12b* enhancer drove expression of *Cre* and *Coup-TF2* (Vogt et al., 2014; Potter et al., 2009). In the control virus, *DlxI12b* drove expression of only *Cre* (*DlxI12b-Cre*). E12.5 *Ai14*$^+$ MGE cells were dissociated and grown *in vitro* for ∼12 h, lentivirus-transduced, grown for 3 days, and then analyzed for *in vitro* expression of tdTomato (induced by Cre), COUP-TF2 and SST. We counted the fraction of tdTomato$^+$ cells (virally transduced) that were COUP-TF2$^+$ and/or SST$^+$ (Fig. S9A,B). Transduction with the control virus produced 27±3% COUP-TF2$^+$; tdTomato$^+$ cells (Fig. S9C); this reflects the fact that dissected MGE had both rostral and caudal parts; only the cMGE has large numbers of COUP-TF2$^+$ cells (Fig. 1A). Transduction with the *Coup-TF2* virus resulted in 2.3-fold more (63±3%) of COUP-TF2$^+$; tdTomato$^+$ cells (Fig. S9C). There was a parallel increase in SST$^+$; tdTomato$^+$ cells and COUP-TF2$^+$; SST$^+$; tdTomato$^+$ cells (Fig. S9C). Thus, *Coup-TF2* transduction was sufficient to induce SST$^+$ fate within 3 days *in vitro*.

To assess whether this fate change persisted *in vivo*, and to examine the effect of *Coup-TF2* expression on the SST$^+$/PV$^+$ ratio, we transplanted dissociated E12.5 MGE cells that had been exposed to either the *Coup-TF2* or control lentiviruses into wild-type P1 neocortex. At P28, we found that *Coup-TF2* transduction increased the SST$^+$/PV$^+$ ratio twofold (Fig. 6H; Fig. S8E-J). In addition, there were increased tdTomato$^+$ cells in layer V (Fig. 6K). Thus *Coup-TF2* was sufficient to increase SST and decrease PV expression cell autonomously.

Together, the results from the *Coup-TF2 in vivo* mutant analysis, the MGE transplantation assay and the *Coup-TF2* transduction experiment show that *Coup-TF2* cell-autonomously promotes the generation of SST$^+$ interneurons and represses the PV$^+$ fate. Furthermore, both assays provide evidence that *Coup-TF2* promotes layer V identity in SST$^+$ CINs.

Coup-TF2 directly binds and activates expression from the *Sox6* locus

As *Coup-TF2* loss *in vivo* led to reduced *Npas1* and *Sox6* expression (Fig. 7A,B; Fig. S3H,I), we tested whether *Coup-TF2*-transduced and -transplanted MGE cells had increased numbers of Npas1$^+$ and Sox6$^+$ cells. Indeed, *Coup-TF2* transduction increased the numbers of cells expressing *Npas1* (2.1-fold) and *Sox6* (1.4-fold) (Fig. 6I,J).

We recently identified an enhancer-like element near *Sox6*, named hs692 (chr7:122,274,934-122,276,253), that has activity in the mantle zone of the MGE and POA (Fig. 7D) (Nord et al., 2013). To test whether COUP-TF2 directly binds to hs692, we performed a ChIP-qPCR from E12.5 MGE, CGE and POA, and found an ∼8-fold enrichment compared with control (mouse IgG) (Fig. 7C). Next, we generated a stable transgenic line in which hs692 drives expression of GFP (Silberberg et al., 2016), and crossed it to the

Development (2017) 144, 2837-2851 doi:10.1242/dev.150664

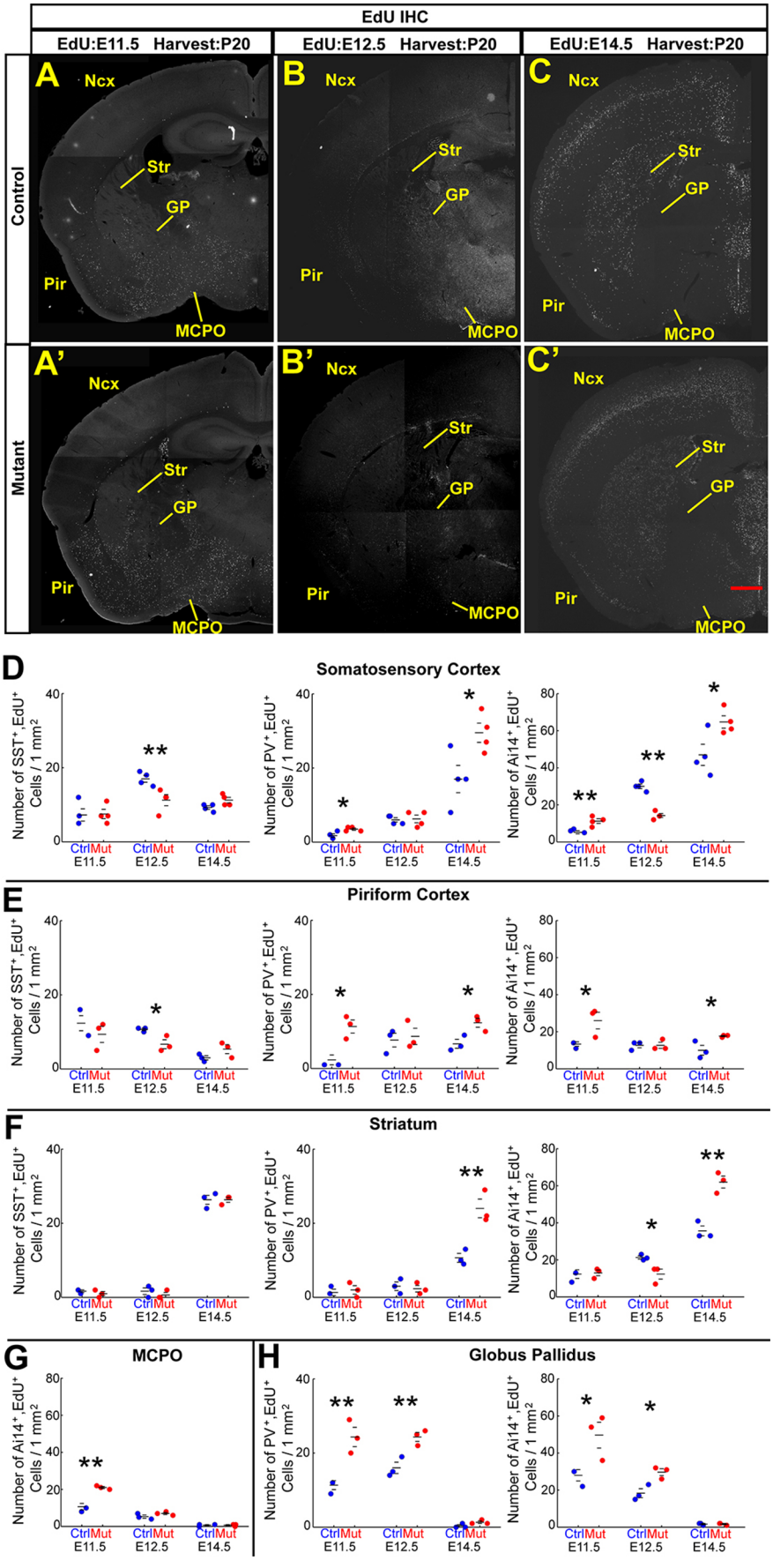

Fig. 5. Loss of *Coup-TF2* affects the numbers of PV$^+$ and SST$^+$ MGE-derived neurons that become postmitotic at specific ages. EdU immunohistochemistry on coronal P20 control (A-C) and mutant (A′-C′) hemisections from mice injected with EdU at E11.5 (A,A′), E12.5 (B,B′) and E14.5 (C,C′) (n=3 for each control and mutant for each age; experiment replicated twice for each age). Scale bar: 500 µm. (D-G) Quantification of EdU$^+$ cells that are SST$^+$, PV$^+$ and tdTomato$^+$ in P20 somatosensory cortex (D), piriform cortex (E), striatum (F), MCPO (G) and globus pallidus (H) from mice injected with EdU at E11.5, E12.5 or E14.5; control (blue) and *Coup-TF2*-sensitized mutant (red). Data are mean±s.e.m. Student's t-test. *P<0.05; **P<0.01. [Also see Fig. S7.] GP, globus pallidus; MCPO, magnocellular preoptic nucleus; Ncx, neocortex; Pir, piriform cortex; Str, striatum.

Development (2017) 144, 2837-2851 doi:10.1242/dev.150664

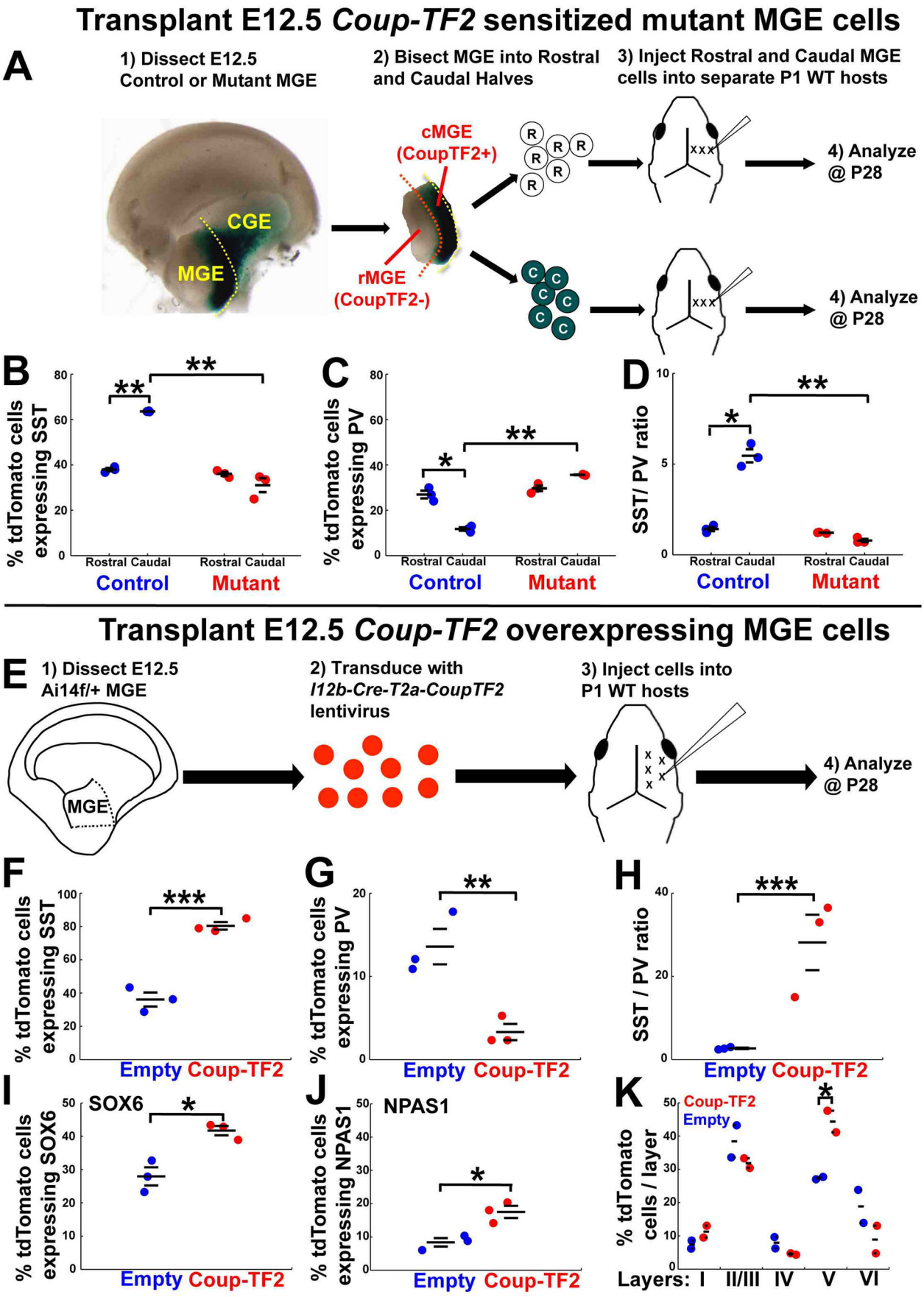

Fig. 6. See next page for legend.

Development (2017) 144, 2837-2851 doi:10.1242/dev.150664

Fig. 6. MGE transplantation into the cortex demonstrates that the rostral and caudal MGE produce different SST$^+$/PV$^+$ ratios that are cell-autonomously regulated by *Coup-TF2*. (A) E12.5 control and mutant MGE tissues are bisected into rostral (enriched with cells lacking *Coup-TF2*) and caudal (enriched with *Coup-TF2*$^+$ cells) halves, and dissociated and transplanted into the cortex of P1 wild-type hosts. tdTomato$^+$ cells are assessed at 27 days post-transplant (DPT) for SST or PV expression. X-gal-stained E12.5 whole-mount (medial view) of an *Nkx2.1-Cre*$^+$*; Coup-TF2*$^{lox/+}$ right telencephalon. Yellow dashed line indicates where the MGE was dissected from the telencephalon. Red dashed line indicates where rostral and caudal MGE were separated. Rostral (R) and caudal (C) MGE cells are indicated in white and green, respectively. (B,C) Proportion of tdTomato$^+$ cells expressing SST (B) and PV (C) from MGE transplants: rostral control (left blue), caudal control (right blue), rostral mutant (left red) or caudal mutant (right red) (n=3 for each control and mutant; experiment replicated twice). (D) The SST$^+$/PV$^+$ ratio for each condition. (E) E12.5 *Ai14*$^{lox/+}$ whole MGE cells were transduced with viruses expressing coding regions for *Cre* only or for *Cre* and *Coup-TF2*, and transplanted into P1 wild-type hosts. tdTomato$^+$ cells are assessed at 27 DPT for SST, PV, SOX6 and NPAS1 expression. (F-H) The proportion of tdTomato$^+$ cells expressing SST (F), PV (G), SOX6 (I) and NPAS1 (J) for MGE transplants transduced with control (blue) or *Coup-TF2* (red) virus (n=3 for each empty vector and Coup-TF2 condition; experiment replicated twice). (H) SST$^+$/PV$^+$ ratio for each condition. (K) Quantification tdTomato$^+$ cells transduced with control or *Coup-TF2* virus in each layer at 27 DPT. Data are mean±s.e.m. Student's t-test (D,H) or χ^2 test (B,C,F,G,I,J,K). *P<0.05; **P<0.01; ***P<0.001. [Also see Fig. S8.] CGE, caudal ganglionic eminence; cMGE, caudal medial ganglionic eminence; rMGE, rostral medial ganglionic eminence.

Coup-TF2-sensitized mutant. In the mutant, there was reduced GFP expression in the MGE and POA MZ (Fig. 7D′). Together, these data provide evidence that COUP-TF2 directly binds to an enhancer near *Sox6*, where it promotes expression in the MGE and POA.

Sox6 transduction rescues the SST$^+$/PV$^+$ ratio phenotype in *Coup-TF2* mutants

As *Coup-TF2* is necessary and sufficient to promote *Sox6* expression, we examined whether *Sox6* could rescue the SST$^+$/PV$^+$ ratio phenotype in *Coup-TF2*-sensitized mutants. We transduced E12.5 caudal control or mutant dissociated MGE cells with a *Dlx12b-GFP-T2a-Sox6* lentivirus (Fig. 7E). Transplanted interneurons transduced with *Sox6* were tdTomato$^+$ (driven by *Nkx2.1-Cre*) and GFP$^+$. Interneurons that were not transduced with *Sox6* (tdTomato$^+$, but GFP$^-$) were used as internal controls.

Sox6 transduction in control cMGE cells increased the SST$^+$/PV$^+$ ratio 2.7-fold, by increasing the number of SST$^+$ interneurons and decreasing the number of PV$^+$ cells (Fig. 7F-H; Fig. S10). In *Coup-TF2*-sensitized mutant cMGE cells, *Sox6* transduction increased the SST$^+$/PV$^+$ ratio 5.1-fold, also by increasing the number of SST$^+$ interneurons and reducing the number of PV$^+$ cells. This provides evidence that *Coup-TF2* regulates the SST$^+$/PV$^+$ ratio through *Sox6*.

DISCUSSION

Regional and cell-type specification during embryogenesis are often coupled to expression of TFs that are restricted to specific progenitor domains. Here, we found that *Nkx2-1* restricts the expression of *Coup-TF1/2* in the MGE to an arc that extended from a small rostrodorsal domain to a larger caudoventral domain (Fig. 1; Fig. S1B,D,H,K,L). The *Coup-TF1/2*$^+$ MGE domain was complementary to an *Otx2*$^+$ domain (Fig. S1B-E), where *Otx2* represses *Coup-TF1* MGE expression (Hoch et al., 2015a,b).

Our data support a model in which the *Coup-TF1/2*$^+$ MGE domain is biased towards generating SST$^+$ CINs (Fig. 2; Fig. S3A-C), as well as cholinergic and pallidal neurons (Fig. S4). These conclusions differ from other publications regarding the major location for the origin of SST$^+$ interneurons, and provide evidence for a *Coup-TF1/2*-dependent activation of *Sox6* expression that promotes SST$^+$ interneuron development.

Multiple lines of evidence show that *Coup-TF1/2* have key roles in promoting SST$^+$ interneuron development. Previously, layer V SST$^+$ CINs were shown to express COUP-TF2 (Cai et al., 2013). Here we demonstrate that *Coup-TF2*-sensitized mutants (*in vivo* genetics and MGE-transplant experiments) have a reduced neocortical SST$^+$/PV$^+$ ratio (Fig. 2A-C). *Coup-TF1/2*-mediated regulation of SST fate operates in MGE progenitors, as we only see the reduced SST$^+$/PV$^+$ ratio using *Nkx2.1-Cre* and not *SST-Cre* (Fig. 3), the latter is only active postmitotically (Taniguchi et al., 2011). *Coup-TF2* sensitized mutants have reduced SST expression in the MGE at E12.5, supporting the early function of these TFs in this cell type (Fig. 2D-G).

We propose that *Coup-TF1/2* promote SST$^+$ interneuron development based on three lines of evidence. First, they promote the survival of SST$^+$ interneuron progenitors, as apoptosis occurs in E11.5 and E12.5 MGE progenitors in *Coup-TF2*-sensitized mutants (Fig. 4A,C; Fig. S5A). Second, *Coup-TF1/2* regulates MGE differentiation and cell cycle dynamics; the mutant MGE has precocious neurogenesis and increased proliferation (Fig. 4B,D-F; Fig. S5B-D). Third, *Coup-TF1/2* specifies SST$^+$ and represses PV$^+$ interneuron fates, as lentiviral transduction of *Coup-TF2* into MGE cells increased the SST$^+$/PV$^+$ ratio (Fig. 6F-H; Figs S8 and 9). It does this by repressing *Ccnd2*, and by promoting *Sox6*, *Lhx6* and *Npas1* expression (Fig. 4F-G′; Fig. S3).

SST$^+$ interneurons are present in cortical layers VI-II. We show that *Coup-TF2*-sensitized mutants had reduced SST$^+$ CINs specifically in layer V (Fig. 2C). Furthermore, in the mutants, there was a reduction in the number of SST$^+$ CIN labeled with EdU at E12.5, a peak age in the generation of layer V CINs (Fig. 5; Fig. S7). On the other hand, the numbers of SST$^+$ CINs labeled with EdU at E11.5 or E14.5 did not change. Lentiviral transduction of *Coup-TF2* in MGE cells, followed by their transplantation, biased the interneurons to acquire layer V identity (Fig. 6K). Together, these data support our hypothesis that *Coup-TF2* contributes to the specification of layer V SST$^+$ CINs. Moreover, the presence of a CIN lamination phenotype in mutants that used *Nkx2.1-Cre* but not with those using *Somatostatin-IRES-Cre* (Fig. 3C-E,J) shows that *Coup-TF1/2*-mediated regulation of layer identity occurs in MGE progenitors and not in immature neurons.

We show that the cMGE is a major contributor of cortical SST$^+$ interneurons. This area had more expansive *Coup-TF1/2* expression than the rostral MGE, and it produced more SST$^+$ than PV$^+$ interneurons in MGE transplantation experiments (Fig. 6B-D). By contrast, the rostral MGE produced more PV$^+$ than SST$^+$ interneurons than the cMGE (Fig. 6B-D); this property was reversed in the *Coup-TF2*-sensitized mutants (Fig. 6B-D). Furthermore, the *Coup-TF2*-sensitized mutants had stronger phenotypes in the caudal basal ganglia, including reduced numbers of *Nkx2.1-Cre* lineage cells (Ai14$^+$) leaving the cMGE (Fig. 1D,E,H), and reduced expression of *Sst*, *Lhx6*, and *Sox6* in the cMGE and CGE (Fig. 2D-G; Fig. S3). By 17.5, mutants showed reduced expression of *Npas1* (Fig. S3H,I), a TF that marks SST$^+$ and not PV$^+$ interneurons, and that positively regulates SST$^+$ interneuron numbers (Stanco et al., 2014).

The dMGE has been proposed to be a major source of SST$^+$ interneurons (Flames et al., 2007; Wonders et al., 2008; Inan et al., 2012). Furthermore, *Nkx6.2-Cre* and *Nkx6.2-Cre*^{ER} fate mapping and *Nkx6.2* functional analyses support the observation that ∼45% of SST$^+$ interneurons are generated by the *Nkx6.2*$^+$ dMGE (Fogarty et al., 2007; Sousa et al., 2009). There is evidence that the dMGE

Development (2017) 144, 2837-2851 doi:10.1242/dev.150664

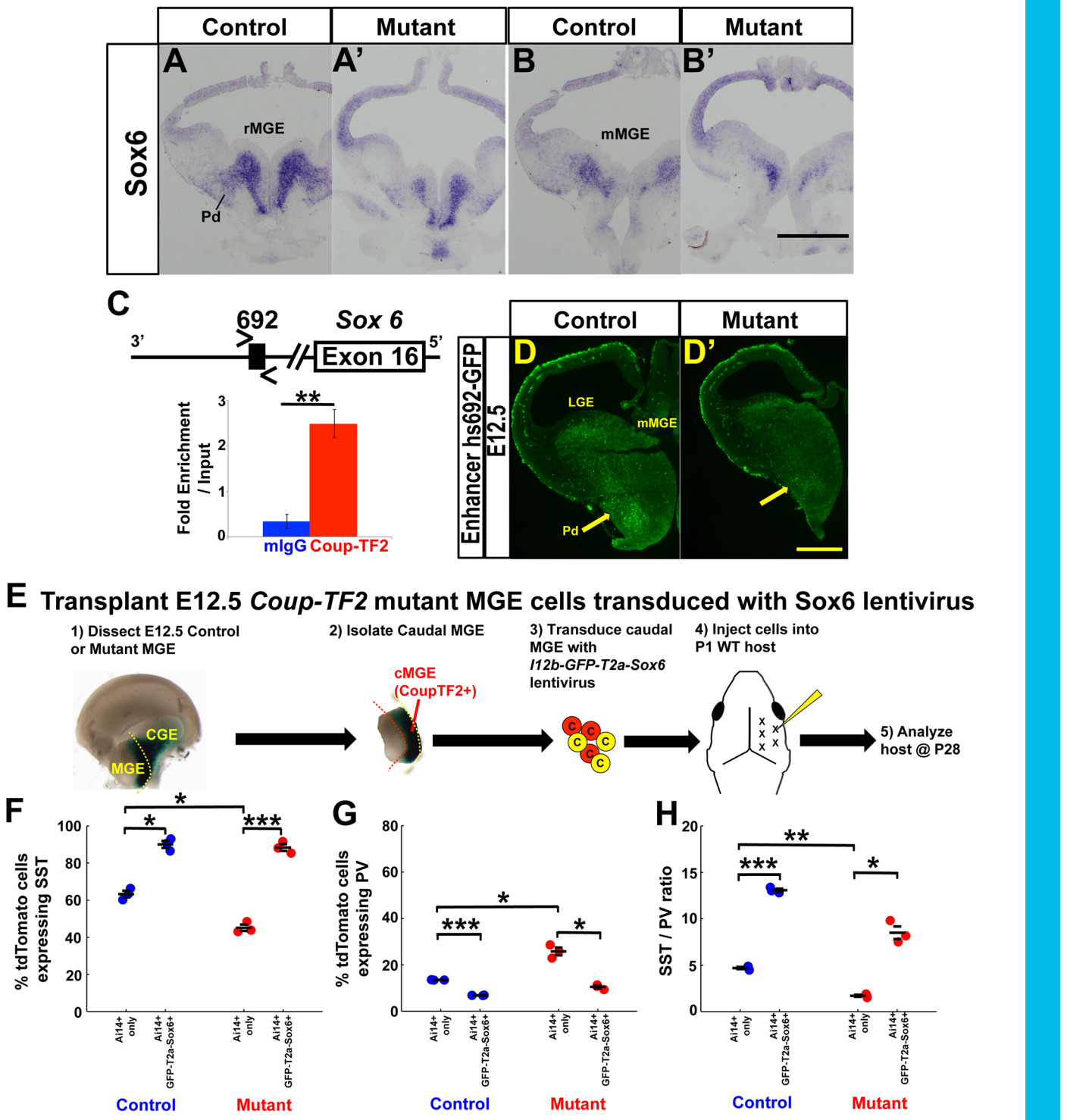

Fig. 7. COUP-TF2 binds to an enhancer near *Sox6* and *Sox6* transduction rescues the SST$^+$/PV$^+$ ratio in the *Coup-TF2*-sensitized mutant. (A-B′) *Sox6 in situ* hybridization of E12.5 control (A,B) and *Coup-TF2*-sensitized mutant (A′,B′) coronal hemisections in two rostral-caudal planes (n=3 for each control and mutant). Scale bar: 1 mm. (C) Schematic of the candidate enhancer region (between > and <) in relation to exon 16 of *Sox6*. Graph shows COUP-TF2 ChIP-qPCR assay results for candidate enhancer region near *Sox6* (n=2 for each mIgG and Coup-TF2 group). (D,D′) GFP immunohistochemistry on E12.5 control (D) and *Coup-TF2*-sensitized mutant (D′) coronal sections comparing GFP levels reporting hs692 enhancer activity (n=2 for each control and mutant). GFP levels are reduced in the MGE MZ (arrow). Scale bar: 500 µm. (E) E12.5 control and mutant cMGE tissues were isolated, transduced with virus encoding *GFP* and *Sox6*, and transplanted into P1 wild-type hosts. Ai14$^+$ cells are assessed at 27 days post-transplant (DPT) for SST or PV expression. Yellow dashed line indicates where MGE was dissected from the telencephalon. Red dashed line indicates where the rostral and caudal MGE were separated. Caudal MGE cells (C) that were or were not transduced with virus are indicated in yellow and red, respectively. (F-H) The proportion of tdTomato$^+$ cells expressing SST (F) and PV (G) for non-transduced control (left, blue), transduced control (right, blue), non-transduced mutant (left, red) or transduced mutant (right, red) caudal MGE transplants (n=3 for each control and mutant; experiment replicated twice). (H) The SST$^+$/PV$^+$ ratio for each condition. Data are mean±s.e.m. χ^2 test (F,G), Student's t-test (H) or Mann–Whitney (C). *P<0.05; **P<0.01; ***P<0.001. [Also see Fig. S10.] CGE, caudal ganglionic eminence; LGE, lateral ganglionic eminence; Pd, pallidum; cMGE, caudal medial ganglionic eminence; mMGE, middle medial ganglionic eminence; rMGE, rostral medial ganglionic eminence.

Development (2017) 144, 2837-2851 doi:10.1242/dev.150664

promotes SST$^+$ generation due to high SHH signaling levels (Xu et al., 2010). Our results do not contradict these ideas, as *Coup-TF1/2* are expressed in the rdMGE. However, our transplantation analyses provide evidence for another major source of SST$^+$ interneurons: the caudal *Coup-TF1/2*$^+$ domain (Fig. 6B-D). Thus, based on *Nkx6.2-Cre* fate mapping (Fogarty et al., 2007) and our transplantation data, we propose that: (1) the cMGE generates at least 30% of SST$^+$ interneurons; (2) PV$^+$ interneurons are primarily generated from *Coup-TF1/2*-negative MGE progenitors, which is primarily the *Otx2*$^+$ rostral MGE domain; and (3) *Coup-TF1/2* promote layer V SST$^+$ CINs.

We hypothesize that *Coup-TF1/2* control the temporal generation of SST versus PV neurons by regulating cell cycle dynamics. At E11.5, *Coup-TF1/2* repress both cell cycle exit and PV$^+$ interneuron fate, based on the findings that: (1) E11.5 *Coup-TF1/2*-sensitized mutants exhibited precocious neurogenesis; and (2) P20 mutants had increased numbers of PV$^+$ neurons in the neocortex, piriform cortex and globus pallidus that were EdU$^+$ (labeled at E11.5) (Fig. 5; Fig. S7). At E12.5, *Coup-TF1/2* promoted SST fate because: (1) E11.5 mutants had progenitor apoptosis and premature neurogenesis, which together could deplete the progenitor pool and neuronal generation at E12.5, including SST$^+$ CINs (Fig. 5); and (2) more E12.5 mutant progenitors remained in the cell cycle (Fig. 4D,E), which subsequently (at E14.5) led to increased numbers of PV$^+$ neurons in the neocortex, piriform cortex and striatum (Fig. 5).

Reduced *Sox6* expression in *Coup-TF2*-sensitized mutants (Fig. 7A-B′) suggests that *Sox6* is an essential component of the transcriptional program of COUP-TF1/2. ChIP-qPCR provided evidence that COUP-TF2 directly binds near the *Sox6* locus (Fig. 7C). We generated a mouse line with a *Sox6* candidate enhancer (hs692) transgene (https://enhancer.lbl.gov). The transcriptional activity of enhancer hs692 in the MGE MZ was reduced in *Coup-TF2*-sensitized mutants (Fig. 7D), supporting the evidence that *Coup-TF1/2* directly regulates this enhancer. Furthermore, *Sox6* transduction rescued the reduced SST$^+$/PV$^+$ ratio in *Coup-TF2*-sensitized mutants (Fig. 7F-H). Previous *Sox6*$^{-/-}$ mutant analysis has shown that it regulates the SST and PV interneuron maturation and does not regulate proliferation and apoptosis in MGE progenitors (Azim et al., 2009; Batista-Brito et al., 2009).

These studies add basic information for elucidating the transcriptional network orchestrating MGE development. *Nkx2.1* and *Otx2* regulate regional fate in the VZ (Corbin et al., 2003; Hoch et al., 2015a,b). *Nkx2.1* represses LGE/CGE and POA fate (Sussel et al., 1999; Flandin et al., 2010), and initiates *Lhx6* and *Lhx8* expression (Sussel et al., 1999; Marin et al., 2000; Du et al., 2008; Flandin et al., 2010). *Lhx6* and *Lhx8* drive differentiation of SST$^+$ and PV$^+$ interneurons, GP and subpallial cholinergic neurons (Rubenstein and Campbell, 2013). *Otx2* specifies ventral MGE identity by repressing POA fate, and promotes early neural and oligodendroctye differentiation (Hoch et al., 2015a,b). *Coup-TF1/2* also function in MGE progenitors, where they specify SST$^+$ and repress PV$^+$ fate in CINs (Fig. 2); they perform this by promoting *Sox6* expression. *Coup-TF1/2* are upstream of *Gbx2* and *Lhx8*, which drive ChAT$^+$ neuron development (Fig. S4D-O) (Rubenstein and Campbell, 2013).

Coup-TF1/2 are the first TFs shown to specify SST$^+$ versus PV$^+$ identity. In addition, other mechanisms are known to control SST$^+$/PV$^+$ ratios (Table S1). For example, there is evidence that these interneuron subtypes can be generated from the same neuroepithelial stem cell, but that some stem cells may produce one subtype (Brown et al., 2011; Ciceri et al., 2013). There is also evidence that these subtypes are generated based on their neurogenic location, where apical progenitors give rise to SST$^+$ and basal progenitors give rise to PV$^+$ interneurons (Petros et al., 2015). Thus, it will be important to learn whether *Coup-TF1/2* expression is enriched in SST$^+$ interneuron-generating stem cells and apical progenitors. *Ccnd2* mutants have an increased SST$^+$/PV$^+$ ratio due to a reduction in PV$^+$ interneuron numbers; the expression of *Ccnd2* is repressed by *Coup-TF1/2* (Fig. 4F,G).

Alterations in CIN subtype numbers have been reported in post-mortem brains from individuals with holoprosencephaly (Fertuzinhos et al., 2009) and neuropsychiatric disorders, and in mouse models of autism spectrum disorder and schizophrenia (Marin, 2012). We suggest that the SST$^+$/PV$^+$ ratio should be measured in these individuals, as mutations in genes associated with neuropsychiatric disorders (*NPAS3* and *PTEN*) alter the SST$^+$/PV$^+$ ratio in mice with mutations of these genes (Vogt et al., 2015; Stanco et al., 2014). Moreover, circuit-level changes, such as gamma oscillations, which is a feature of schizophrenia, have been observed in *PTEN* mouse mutants (Stanco et al., 2014).

MATERIALS AND METHODS

Mice

The following mouse strains have been previously reported: *tdTomato*$^{lox/+}$ (Ai14) Cre-reporter (Madisen et al., 2010), *Coup-TF1*$^{+/-}$ (Qiu et al., 1997), *Coup-TF2*$^{lox/+}$ (Takamoto et al., 2005), *Nkx2.1*$^{lox/+}$ *Dlx1-CreERT* (Taniguchi et al., 2011), *Olig2-Cre*, *Somatostatin-IRES-Cre* (Taniguchi et al., 2011), *Nkx2.1-Cre* (Xu et al., 2008) and *hs692-GFP* (Silberberg et al., 2016). All strains were on a C57BL/6 background. P1 wild-type hosts (Figs 6 and 7C-F) were CD-1 (Charles River Laboratories). All animals were housed in a vivarium with a 12 h light/12 h dark cycle. Postnatal animals used for experiments were kept with their littermates. Males and females were both used in all experiments.

For timed pregnancies, noon on the day of the vaginal plug was counted as embryonic day (E) 0.5. For EdU experiments, pregnant mice were injected with a single dose of 50 mg/kg body weight (from a 10 mg/ml stock) intraperitoneally, and brains were harvested 1 (Fig. S13), 5 hours (Fig. 4; Fig. S5) or 24 h (Fig. S11) later or at P20 (Fig. 5; Fig. S7). For tamoxifen experiments, pregnant mice were administered 2 mg/40 kg body weight (from a 10 mg/ml stock dissolved in corn oil) by oral gavaging with silicon-protected needles. All animal care and procedures were performed according to the University of California at San Francisco Laboratory Animal Research Center guidelines. Mice were euthanized with CO_2 inhalation followed by cervical dislocation. Isolated brains that were used for *in situ* hybridization and immunohistochemistry were fixed overnight in 4% paraformaldehyde (PFA), transferred to 30% sucrose overnight for cryoprotection, and then OCT embedded for cryosectioning. Sections were cut coronally at 20 µm. For postnatal experiments, animals were anesthetized with intraperitoneal avertin (0.015 ml/g of a 2.5% solution) and perfused transcardially with PBS and then with 4% PFA, followed by brain isolation, overnight fixation, 2 days of cryoprotection and microtome sectioning (coronal, 40 µm).

Antibodies and reagents

Antibodies used were rabbit cC3 (1:250, 9661S, Cell Signaling), mouse Coup-TF2 (1:350, PP-H7147-00, Perseus Proteomics), rabbit DsRed (1:500, 632496, Clontech), chicken GFP (1:500, GFP1020, Aves), rabbit ki67 (1:250, 16667, Abcam), mouse parvalbumin (1:300, MAB1572, Swant Swiss Abs), rabbit pH3 (1:500, 06-750, Upstate), rat somatostatin (1:200, MAB354, Chemicon), goat somatostatin (1:100, SC-7819, Santa Cruz), mouse TuJ1 (1:1000, MMS-435P, Covance), goat ChAT (1:100, AB144P, Millipore) and Alexa-conjugated secondary antibodies (1:300, Molecular Probes). Sections were cover slipped with Vectashield containing DAPI (Vector labs). For antibody validation references, see supplementary Materials and Methods.

In situ hybridization

We performed *in situ* hybridization on a minimum of n=3 biological replicates for each control and mutant. In each case, a rostrocaudal series of

Development (2017) 144, 2837-2851 doi:10.1242/dev.150664

at least ten sections was examined. *In situ* hybridizations were performed using digoxigenin-labeled riboprobes as described previously (Hoch et al., 2015a,b).

Immunohistochemistry

cC3, dsRed, GFP, ki67, pH3 and TuJ1 immunohistochemistry on embryonic brains was performed on slide-mounted cryosections. These were rinsed in phosphate-buffered saline (PBS), blocked in 10% normal serum/PBST (PBS with 0.1% Triton X-100), incubated in primary antibody overnight (4°C), washed in PBST, incubated with secondary antibody for 1-2 h (at room temperature) and washed in PBS. For COUP-TF2, immunohistochemistry was performed as described above but with antigen retrieval [20 min boiling in 10 mM sodium citrate and 0.05% Tween 20 (pH 6), cooled at room temperature for 20 min] and immunoperoxidase staining with ImmPRESS reagent kit (Vector Laboratories). For EdU IHC, EdU was labeled with a Click-iT EdU Alexa Fluor Imaging kit (Catalog #C10337, Molecular Probes).

ChAT IHC on postnatal brains was performed as described (Hoch et al., 2015a,b). For all immunohistochemistry on postnatal brains, staining was carried out on free-floating sections as described previously (Stanco et al., 2014). We performed all immunohistochemistry on $n \geq 3$ biological replicates for each control and mutant, except for Fig. 7D ($n=2$ biological replicates).

Whole-mount X-gal staining

We performed whole-mount X-gal staining on E12.5 brains from *Nkx2.1-Cre*$^{+}$; *Coup-TF2*$^{lox/+}$ embryos to report expression of *Coup-TF2* in MGE/POA. A Cre recombination reporter was used: *lacZ* (encoding βgal) located 3′ of the floxed region in the Coup-TF2^{lox} allele. Its expression is activated upon Cre-mediated recombination. Brains were isolated from E12.5 embryos and rinsed in PBS, fixed in 2% PFA and 0.2% glutaraldehyde for 1 h, rinsed again in PBS and stained overnight at 37°C with 1 mg/ml X-gal, 5 mM potassium ferricyanide, 5 mM potassium ferrocyanide, 2 mM $MgCl_2$, 0.01% sodium deoxycholate, and 0.02% nonidet P-40 in PBS. The reaction was stopped with a PBS wash, 4% PFA postfix and another PBS wash.

MGE transplantation and transduction, and lentiviral production

For experiments involving *Coup-TF2*-sensitized mutant MGE transplants (Figs 6A-D and 7C-F; Figs S8A-D and S10), MGEs were split into rostral and caudal halves. For experiments involving *COUP-TF2*-transduced MGE transplants (Fig. 6E-K; Fig. S8E-J), whole MGEs were used. Transplantation, transduction and lentiviral production were performed as described previously (Vogt et al., 2014).

Lentiviral vector generation

Generation of the *DlxI12b-GFP-T2a-Sox6* lentiviral vector has been reported previously (Vogt et al., 2014). For the *DlxI12b-Cre-T2a-CoupTF2* lentiviral vector, a human full-length *COUP-TF2* was PCR amplified with *Eco*RI and *Age*I sites introduced on the 5′ and 3′ ends, respectively, from a pcDNA5/FRT/TO vector (5′GAGAGAATTCAAGCT-TGCCACCATGGCC, 3′GAGAACCGGTTTATTGAATTGCCATATA) (the vector was a gift from Ming-Jer Tsai and Sophia Tsai, Baylor College of Medicine, TX, USA). The PCR product was cloned in frame, 3′ to the T2a sequence of a *CMV-GFP-T2a-mcs* vector. Next, the *T2a-CoupTF2* was isolated from this vector by digestion with *Bsr*GI and *Sac*II; it was then ligated into a *DlxI12b-Cre-T2a-mcs* vector (also digested with *Bsr*GI and *Sac*II to remove the T2a-mcs site) 3′ to the *Cre* gene. All vectors were verified by sequencing.

Primary cell culture

MGE tissue was dissected from E12.5 *Ai14*$^{lox/+}$ embryos and mechanically dissociated using a P1000 pipette tip. Two hundred thousand cells were seeded onto tissue-culture slides precoated with poly-L-lysine (10 mg/ml, Sigma) and laminin (5 mg/ml, Sigma), and grown *in vitro* with DMEM-H21 media with 10% fetal bovine serum for ∼12 h. MGE primary cultures were then transduced with lentivirus for 30 min at 37°C. Cultures were washed and grown for 3 days in Neurobasal medium containing B27 supplement, 25% glucose and glutamax. Cultures were fixed with 4% PFA for 10 min and processed for immunocytochemistry as follows: washed in PBS, blocked in 5% bovine serum albumin/PBST, incubated in primary antibody overnight (4°C), washed in PBS, incubated in secondary antibody for 1-2 h (at room temperature), washed in PBS and mounted.

Image acquisition and analysis

Fluorescent images were taken using a Coolsnap camera (Photometrics) mounted on a Nikon Eclipse 80i microscope using NIS Elements acquisition software (Nikon). Bright-field images were taken using a DP70 camera (Olympus) mounted on an Olympus SZX7 microscope. Brightness and contrast were adjusted and images merged using ImageJ software.

Cell counting

For assessing cell densities, 10× images were taken at the somatosensory cortex, piriform cortex, striatum, magnocellular preoptic nucleus or globus pallidus at embryonic or postnatal ages from two or three nonadjacent sections and from both hemispheres for each replicate. A box of a defined area was drawn over a region of interest. Cells were counted within that box and were divided by the box area. For lamination counts, we used DAPI to subdivide neocortical layers. Counting of transplanted MGE cells were performed as described previously (Vogt et al., 2014). See supplementary Materials and Methods for details.

For cC3, EdU, Ki67, pH3 and TuJ1 MGE counts, a 0.17 mm×0.25 mm box was drawn for all ages on the rostral dorsal, caudal and rostral ventral MGE regions. Boxes were placed based on COUP-TF2 expression in adjacent sections. The VZ and SVZ boundary was drawn based on DAPI staining. The SVZ1/SVZ2 boundary was drawn across half of the SVZ subregion. All counts were carried out in these three regions within the box. The Q fraction was the number of cells that were double positive for TuJ1 and EdU, divided by the total number of EdU^{+} cells. The P fraction was the numbers of cells that were double positive for Ki67 and EdU, divided by the total number of Ki67^{+} cells.

Statistics

No statistical methods were used to predetermine sample size. Number of replicates was limited by the probability of generating mutants from a given cross. Sample sizes mentioned above were deemed adequate as reported phenotypes were clear and seen in all replicates. Moreover, most phenotypes were quantified and statistically tested to see if these were real.

All statistical analyses were carried out on SPSS15 software except for the χ^2 test (Microsoft Excel). All data points except for ChIP-qPCR data (Fig. 7C) were found to lie within a normal distribution using a Shapiro-Wilk test, and were therefore suitable for parametric testing. All data groups were determined to have equal variance as analyzed by Levene's test. For cell density data, significance was determined using Student's *t*-test as groups lie within a normal distribution and have equal variance. For transplant data and layer counting, significance was determined by χ^2 test. For determining significance in the ChIP-qPCR data (Fig. 7C), we used a Mann–Whitney test (nonparametric) as $n=2$. All data except for ChIP-qPCR (Fig. 7C) were collected and processed blindly during the data analysis. No data were randomized.

Chromatin immunoprecipitation and qPCR

Chromatin immunoprecipitation (ChIP) (according to Millipore-Upstate ChIP protocol) was performed on E12.5 wild-type CD1 MGE, CGE and POA tissues, which were fixed in 1.5% formaldehyde for 20 min at room temperature and then neutralized with glycine. The cross-linked chromatin was sheared using a Bioruptor UCD-200 for 40 cycles (1 round=30 s on/45 s off at high intensity). The sheared chromatin was incubated at 4°C overnight with 5 µg of mouse COUP-TF2 monoclonal antibody (Perseus Proteomics, PP-H7147-00) or 5 µg mouse IgG (Santa Cruz, SC-2025) as a negative control. Protein/antibody complexes were collected using Dynabeads (20 µl protein A+20 µl protein G, Invitrogen), washed and eluted.

ChIP-qPCR analysis was performed on a 7900HT Fast Real-Time PCR System (Applied Biosystems) using SYBR GreenER qPCR SuperMix

Development (2017) 144, 2837-2851 doi:10.1242/dev.150664

(Invitrogen), and qPCR data were analyzed as described by Vokes et al. (2007). For each condition, n=2 biological replicates tested. The following qPCR primers were used to detect enhancer hs692 (near *Sox6*): forward, CACGGGGCCAGATCTAGTTA; reverse, CACCATTGTTACCCGCCTAT.

Acknowledgements

We are grateful to Ke Tang, Ming-Jer Tsai and Sophia Tsai for the *Coup-TF1*$^{+/-}$ and *Coup-TF2*$^{lox/+}$ mice, and *Coup-TF2* expression construct. We are also grateful to members of the Rubenstein Lab for insightful comments and feedback.

Competing interests

J.L.R.R. is a co-founder and stockholder, and is currently on the scientific board of *Neurona*, a company studying the potential therapeutic use of interneuron transplantation.

Author contributions

Conceptualization: J.S.H., D.V., S.L., J.L.R.R.; Methodology: J.S.H., D.V., S.L., M.S., S.N.S., J.L.R.R.; Validation: J.S.H., D.V., S.L., M.S., S.N.S., J.L.R.R.; Formal analysis: J.S.H., D.V., S.L., M.S., J.L.R.R.; Investigation: J.S.H., D.V., S.L., M.S., J.L.R.R.; Resources: J.S.H., D.V., S.L., M.S., S.N.S., J.L.R.R.; Writing - original draft: J.S.H., J.L.R.R.; Writing - review & editing: J.S.H., J.L.R.R.; Supervision: J.L.R.R.; Project administration: J.L.R.R.; Funding acquisition: J.S.H., J.L.R.R.

Funding

This work was supported by research grants from the National Institute of Mental Health (T32 MH089920 to J.S.H., T32 GM00744 to S.S., and R01 MH081880 and R37 MH049428 to J.L.R.R.) and from the Brain and Behavior Research Foundation (2013 NARSAD Young Investigator Grant to J.S.H.). Deposited in PMC for release after 12 months.

Supplementary information

Supplementary information available online at
http://dev.biologists.org/lookup/doi/10.1242/dev.150664.supplemental

References

Au, E., Ahmed, T., Karayannis, T., Biswas, S., Gan, L. and Fishell, G. (2013). A modular gain-of-function approach to generate cortical interneuron subtypes from ES cells. *Neuron* **80**, 1145-1158.

Azim, E., Jabaudon, D., Fame, R. M. and Macklis, J. D. (2009). SOX6 controls dorsal progenitor identity and interneuron diversity during neocortical development. *Nat. Neurosci.* **12**, 1238-1247.

Batista-Brito, R., Rossignol, E., Hjerling-Leffler, J., Denaxa, M., Wegner, M., Lefebvre, V., Pachnis, V. and Fishell, G. (2009). The cell-intrinsic requirement of Sox6 for cortical interneuron development. *Neuron* **63**, 466-481.

Brown, K. N., Chen, S., Han, Z., Lu, C.-H., Tan, X., Zhang, X.-J., Ding, L., Lopez-Cruz, A., Saur, D., Anderson, S. A. et al. (2011). Clonal production and organization of inhibitory interneurons in the neocortex. *Science* **334**, 480-486.

Cai, Y., Zhang, Q., Wang, C., Zhang, Y., Ma, T., Zhou, X., Tian, M., Rubenstein, J. L. R. and Yang, Z. (2013). Nuclear receptor COUP-TFII-expressing neocortical interneurons are derived from the medial and lateral/caudal ganglionic eminence and define specific subsets of mature interneurons. *J. Comp. Neurol.* **521**, 479-497.

Chen, L., Chatterjee, M. and Li, J. Y. H. (2010). The mouse homeobox gene Gbx2 is required for the development of cholinergic interneurons in the striatum. *J. Neurosci.* **30**, 14824-14834.

Ciceri, G., Dehorter, N., Sols, I., Huang, Z. J., Maravall, M. and Marín, O. (2013). Lineage-specific laminar organization of cortical GABAergic interneurons. *Nat. Neurosci.* **16**, 1199-1210.

Close, J., Xu, H., De Marco García, N., Batista-Brito, R., Rossignol, E., Rudy, B. and Fishell, G. (2012). Satb1 is an activity-modulated transcription factor required for the terminal differentiation and connectivity of medial ganglionic eminence-derived cortical interneurons. *J. Neurosci.* **32**, 17690-17705.

Cobos, I., Calcagnotto, M. E., Vilaythong, A. J., Thwin, M. T., Noebels, J. L., Baraban, S. C. and Rubenstein, J. L. R. (2005). Mice lacking Dlx1 show subtype-specific loss of interneurons, reduced inhibition and epilepsy. *Nat. Neurosci.* **8**, 1059-1068.

Colasante, G., Collombat, P., Raimondi, V., Bonanomi, D., Ferrai, C., Maira, M., Yoshikawa, K., Mansouri, A., Valtorta, F., Rubenstein, J. L. R. et al. (2008). Arx is a direct target of Dlx2 and thereby contributes to the tangential migration of GABAergic interneurons. *J. Neurosci.* **28**, 10674-10686.

Corbin, J. G., Rutlin, M., Gaiano, N. and Fishell, G. (2003). Combinatorial function of the homeodomain proteins Nkx2.1 and Gsh2 in ventral telencephalic patterning. *Development* **130**, 4895-4906.

Du, T., Xu, Q., Ocbina, P. J. and Anderson, S. A. (2008). NKX2.1 specifies cortical interneuron fate by activating Lhx6. *Development* **135**, 1559-1567.

Fertuzinhos, S., Li, M., Kawasawa, Y. I., Ivic, V., Franjic, D., Singh, D., Crair, M. and Sestan, N. (2009). Selective depletion of molecularly defined cortical interneurons in human holoprosencephaly with severe striatal hypoplasia. *Cereb. Cortex* **19**, 2196-2207.

Flames, N., Pla, R., Gelman, D. M., Rubenstein, J. L. R., Puelles, L. and Marín, O. (2007). Delineation of multiple subpallial progenitor domains by the combinatorial expression of transcriptional codes. *J. Neurosci.* **27**, 9682-9695.

Flandin, P., Kimura, S. and Rubenstein, J. L. R. (2010). The progenitor zone of the ventral medial ganglionic eminence requires Nkx2-1 to generate most of the globus pallidus but few neocortical interneurons. *J. Neurosci.* **30**, 2812-2823.

Fogarty, M., Grist, M., Gelman, D., Marín, O., Pachnis, V. and Kessaris, N. (2007). Spatial genetic patterning of the embryonic neuroepithelium generates GABAergic interneuron diversity in the adult cortex. *J. Neurosci.* **27**, 10935-10946.

Glickstein, S. B., Moore, H., Slowinska, B., Racchumi, J., Suh, M., Chuhma, N. and Ross, M. E. (2007). Selective cortical interneuron and GABA deficits in cyclin D2-null mice. *Development* **134**, 4083-4093.

Hoch, R. V., Clarke, J. A. and Rubenstein, J. L. R. (2015a). Fgf signaling controls the telencephalic distribution of Fgf-expressing progenitors generated in the rostral patterning center. *Neural Dev.* **10**, 8.

Hoch, R. V., Lindtner, S., Price, J. D. and Rubenstein, J. L. R. (2015b). OTX2 transcription factor controls regional patterning within the medial ganglionic eminence and regional identity of the septum. *Cell Rep.* **12**, 482-494.

Inan, M., Welagen, J. and Anderson, S. A. (2012). Spatial and temporal bias in the mitotic origins of somatostatin- and parvalbumin-expressing interneuron subgroups and the chandelier subtype in the medial ganglionic eminence. *Cereb. Cortex* **22**, 820-827.

Kanatani, S., Yozu, M., Tabata, H. and Nakajima, K. (2008). COUP-TFII is preferentially expressed in the caudal ganglionic eminence and is involved in the caudal migratory stream. *J. Neurosci.* **28**, 13582-13591.

Kepecs, A. and Fishell, G. (2014). Interneuron cell types are fit to function. *Nature* **505**, 318-326.

Liodis, P., Denaxa, M., Grigoriou, M., Akufo-Addo, C., Yanagawa, Y. and Pachnis, V. (2007). Lhx6 activity is required for the normal migration and. specification of cortical interneuron subtypes. *J. Neurosci.* **27**, 3078-3089.

Lodato, S., Tomassy, G. S., De Leonibus, E., Uzcategui, Y. G., Andolfi, G., Armentano, M., Touzot, A., Gaztelu, J. M., Arlotta, P., Menendez de la Prida, L. et al. (2011). Loss of COUP-TFI alters the balance between caudal ganglionic eminence- and medial ganglionic eminence-derived cortical interneurons and results in resistance to epilepsy. *J. Neurosci.* **31**, 4650-4662.

Madisen, L., Zwingman, T. A., Sunkin, S. M., Oh, S. W., Zariwala, H. A., Gu, H., Ng, L. L., Palmiter, R. D., Hawrylycz, M. J., Jones, A. R. et al. (2010). A robust and high-throughput Cre reporting and characterization system for the whole mouse brain. *Nat. Neurosci.* **13**, 133-140.

Marin, O. (2012). Interneuron dysfunction in psychiatric disorders. *Nat. Rev. Neurosci.* **13**, 107-120.

Marin, O., Anderson, S. A. and Rubenstein, J. L. (2000). Origin and molecular specification of striatal interneurons. *J. Neurosci.* **20**, 6063-6076.

Murayama, M., Pérez-Garci, E., Nevian, T., Bock, T., Senn, W. and Larkum, M. E. (2009). Dendritic encoding of sensory stimuli controlled by deep cortical interneurons. *Nature* **457**, 1137-1141.

Neves, G., Shah, M. M., Liodis, P., Achimastou, A., Denaxa, M., Roalfe, G., Sesay, A., Walker, M. C. and Pachnis, V. (2013). The LIM homeodomain protein Lhx6 regulates maturation of interneurons and network excitability in the mammalian cortex. *Cereb. Cortex* **23**, 1811-1823.

Nord, A. S., Blow, M. J., Attanasio, C., Akiyama, J. A., Holt, A., Hosseini, R., Phouanenavong, S., Plajzer-Frick, I., Shoukry, M., Afzal, V. et al. (2013). Rapid and pervasive changes in genome-wide enhancer usage during mammalian development. *Cell* **155**, 1521-1531.

Petros, T. J., Bultje, R. S., Ross, M. E., Fishell, G. and Anderson, S. A. (2015). Apical versus basal neurogenesis directs cortical interneuron subclass fate. *Cell Rep.* **6**, 1090-1095.

Potter, G. B., Petryniak, M. A., Shevchenko, E., McKinsey, G. L., Ekker, M. and Rubenstein, J. L. R. (2009). Generation of Cre-transgenic mice using Dlx1/Dlx2 enhancers and their characterization in GABAergic interneurons. *Mol. Cell. Neurosci.* **40**, 167-186.

Qiu, Y., Pereira, F. A., DeMayo, F. J., Lydon, J. P., Tsai, S. Y. and Tsai, M.-J. (1997). Null mutation of mCOUP-TFI results in defects in morphogenesis of the glossopharyngeal ganglion, axonal projection, and arborization. *Genes Dev.* **11**, 1925-1937.

Rubenstein, J. L. R. and Campbell, K. (2013). *Neurogenesis in the Basal Ganglia. Patterning and Cell Type Specification in the Developing CNS and PNS: Comprehensive Developmental Neuroscience*, pp. 455-473. London, U.K: Elsevier Inc.

Silberberg, S. N., Taher, L., Lindtner, S., Sandberg, M., Nord, A. S., Vogt, D., Mckinsey, G. L., Hoch, R., Pattabiraman, K., Zhang, D. et al. (2016). subpallial enhancer transgenic lines: a data and tool resource to study transcriptional regulation of GABAergic cell fate. *Neuron* **92**, 59-74.

Silbereis, J. C., Nobuta, H., Tsai, H. H., Heine, V. M., McKinsey, G. L., Meijer, D. H., Howard, M. A., Petryniak, M. A., Potter, G. B., Alberta, J. A. et al. (2014).

Olig1 function is required to repress dlx1/2 and interneuron production in Mammalian brain. *Neuron* **81**, 574-587.

Sohal, V. S., Zhang, F., Yizhar, O. and Deisseroth, K. (2009). Parvalbumin neurons and gamma rhythms enhance cortical circuit performance. *Nature* **459**, 698-702.

Sousa, V. H., Miyoshi, G., Hjerling-Leffler, J., Karayannis, T. and Fishell, G. (2009). Characterization of Nkx6-2-derived neocortical interneuron lineages. *Cereb. Cortex* **19** Suppl. 1, i1-i10.

Stanco, A., Pla, R., Vogt, D., Chen, Y., Mandal, S., Walker, J., Hunt, R. F., Lindtner, S., Erdman, C. A., Pieper, A. A. et al. (2014). NPAS1 represses the generation of specific subtypes of cortical interneurons. *Neuron* **84**, 940-953.

Sussel, L., Marin, O., Kimura, S. and Rubenstein, J. L. (1999). Loss of Nkx2.1 homeobox gene function results in a ventral to dorsal molecular respecification within the basal telencephalon: evidence for a transformation of the pallidum into the striatum. *Development* **126**, 3359-3370.

Takamoto, N., You, L. R., Moses, K., Chiang, C., Zimmer, W. E., Schwartz, R. J., DeMayo, F. J., Tsai, M. J. and Tsai, S. Y. (2005). COUP-TFII is essential for radial and anteroposterior patterning of the stomach. *Development* **132**, 2179-2189.

Tang, K., Xie, X., Park, J.-I., Jamrich, M., Tsai, S. and Tsai, M. J. (2010). COUP-TFs regulate eye development by controlling factors essential for optic vesicle morphogenesis. *Development* **137**, 725-734.

Tang, K., Rubenstein, J. L. R., Tsai, S. Y. and Tsai, M.-J. (2012). COUP-TFII controls amygdala patterning by regulating neuropilin expression. *Development* **139**, 1630-1639.

Taniguchi, H., He, M., Wu, P., Kim, S., Paik, R., Sugino, K., Kvitsiani, D., Fu, Y., Lu, J., Lin, Y. et al. (2011). A resource of Cre driver lines for genetic targeting of GABAergic neurons in cerebral cortex. *Neuron* **71**, 995-1013.

Tripodi, M., Filosa, A., Armentano, M. and Studer, M. (2004). The COUP-TF nuclear receptors regulate cell migration in the mammalian basal forebrain. *Development* **131**, 6119-6129.

Vogt, D., Hunt, R. F., Mandal, S., Sandberg, M., Silberberg, S. N., Nagasawa, T., Yang, Z., Baraban, S. C. and Rubenstein, J. L. R. (2014). Lhx6 directly regulates Arx and CXCR7 to determine cortical interneuron fate and laminar position. *Neuron* **82**, 350-364.

Vogt, D., Cho, K. K. A., Lee, A. T., Sohal, V. S. and Rubenstein, J. L. R. (2015). The parvalbumin/somatostatin ratio is increased in Pten mutant mice and by human PTEN ASD alleles. *Cell Rep.* **11**, 944-956.

Vokes, S. A., Ji, H., McCuine, S., Tenzen, T., Giles, S., Zhong, S., Longabaugh, W. J., Davidson, E. H., Wong, W. H. and McMahon, A. P. (2007). Genomic characterization of Gli-activator targets in sonic hedgehog-mediated neural patterning. *Development* **134**, 1977-1989.

Wang, Y., Dye, C. A., Sohal, V., Long, J. E., Estrada, R. C., Roztocil, T., Lufkin, T., Deisseroth, K., Baraban, S. C. and Rubenstein, J. L. R. (2010). Dlx5 and Dlx6 regulate the development of parvalbumin-expressing cortical interneurons. *J. Neurosci.* **30**, 5334-5345.

Wonders, C. P., Taylor, L., Welagen, J., Mbata, I. C., Xiang, J. Z. and Anderson, S. A. (2008). A spatial bias for the origins of interneuron subgroups within the medial ganglionic eminence. *Dev. Biol.* **314**, 127-136.

Xu, Q., Tam, M. and Anderson, S. A. (2008). Fate mapping Nkx2.1-lineage cells in the mouse telencephalon. *J. Comp. Neurol.* **506**, 16-29.

Xu, Q., Guo, L., Moore, H., Waclaw, R. R., Campbell, K. and Anderson, S. A. (2010). Sonic hedgehog signaling confers ventral telencephalic progenitors with distinct cortical interneuron fates. *Neuron* **65**, 328-340.

Zhao, Y., Marín, O., Hermesz, E., Powell, A., Flames, N., Palkovits, M., Rubenstein, J. L. R. and Westphal, H. (2003). The LIM-homeobox gene Lhx8 is required for the development of many cholinergic neurons in the mouse forebrain. *Proc. Natl. Acad. Sci. USA* **100**, 9005-9010.

Zhao, Y., Flandin, P., Long, J. E., Cuesta, M. D., Westphal, H. and Rubenstein, J. L. R. (2008). Distinct molecular pathways for development of telencephalic interneuron subtypes revealed through analysis of Lhx6 mutants. *J. Comp. Neurol.* **510**, 79-99.

Zhao, Y., Flandin, P., Vogt, D., Blood, A., Hermesz, E., Westphal, H. and Rubenstein, J. L. R. (2014). Ldb1 is essential for development of Nkx2.1 lineage derived GABAergic and cholinergic neurons in the telencephalon. *Dev. Biol.* **385**, 94-106.